EUROPEAN ORGANISATION FOR NUCLEAR RESEARCH

CERN-PPE/94-123

27.07.94

Determination of event shape distributions and α_s^b from $Z^0 \to b\bar{b}$ events at LEP

The OPAL Collaboration

Abstract

In hadronic Z^0 decays collected by the OPAL experiment at LEP, event shape variables such as jet rates, jet masses, thrust and the energy-energy correlation for $Z^0 \to b\bar{b}$ events are compared to those for all flavours using secondary vertex information to tag the b quarks. The measured distributions are found to be well described by an $\mathcal{O}(\alpha_s)$ calculation for heavy quarks as well as by parton shower simulations. We also determine the ratio of the strong coupling constant for b quarks and all quarks, $\alpha_s^b/\alpha_s^{incl}$, from these distributions. We find

$$\alpha_s^b/\alpha_s^{incl} = 0.994 \pm 0.005 \,^{+\,0.010}_{-\,0.012} \quad ,$$

where the errors are the statistical and systematic errors. The result can be converted into the ratio for b quarks relative to the complementary flavours udsc $\alpha_s^b/\alpha_s^{udsc} = 0.992 \pm 0.007 \,^{+\,0.013}_{-\,0.015}$.

To be submitted to Z. Phys. C

The OPAL Collaboration

R. Akers[16], G. Alexander[23], J. Allison[16], K.J. Anderson[9], S. Arcelli[2], S. Asai[24], A. Astbury[28], D. Axen[29], G. Azuelos[18,a], A.H. Ball[17], E. Barberio[26], R.J. Barlow[16], R. Bartoldus[3], J.R. Batley[5], G. Beaudoin[18], A. Beck[23], G.A. Beck[13], J. Becker[10], C. Beeston[16], T. Behnke[27], K.W. Bell[20], G. Bella[23], P. Bentkowski[18], S. Bentvelsen[8], P. Berlich[10], S. Bethke[32], O. Biebel[32], I.J. Bloodworth[1], P. Bock[11], H.M. Bosch[11], M. Boutemeur[18], S. Braibant[12], P. Bright-Thomas[25], R.M. Brown[20], A. Buijs[8], H.J. Burckhart[8], C. Burgard[27], P. Capiluppi[2], R.K. Carnegie[6], A.A. Carter[13], J.R. Carter[5], C.Y. Chang[17], C. Charlesworth[6], D.G. Charlton[8], S.L. Chu[4], P.E.L. Clarke[15], J.C. Clayton[1], S.G. Clowes[16], I. Cohen[23], J.E. Conboy[15], M. Coupland[14], M. Cuffiani[2], S. Dado[22], C. Dallapiccola[17], G.M. Dallavalle[2], C. Darling[31], S. De Jong[13], H. Deng[17], M. Dittmar[4], M.S. Dixit[7], E. do Couto e Silva[12], J.E. Duboscq[8], E. Duchovni[26], G. Duckeck[8], I.P. Duerdoth[16], U.C. Dunwoody[5], P.A. Elcombe[5], P.G. Estabrooks[6], E. Etzion[23], H.G. Evans[9], F. Fabbri[2], B. Fabbro[21], M. Fanti[2], M. Fierro[2], M. Fincke-Keeler[28], H.M. Fischer[3], P. Fischer[3], R. Folman[26], D.G. Fong[17], M. Foucher[17], H. Fukui[24], A. Fürtjes[8], P. Gagnon[6], A. Gaidot[21], J.W. Gary[4], J. Gascon[18], N.I. Geddes[20], C. Geich-Gimbel[3], S.W. Gensler[9], F.X. Gentit[21], T. Geralis[20], G. Giacomelli[2], P. Giacomelli[4], R. Giacomelli[2], V. Gibson[5], W.R. Gibson[13], J.D. Gillies[20], J. Goldberg[22], D.M. Gingrich[30,a], M.J. Goodrick[5], W. Gorn[4], C. Grandi[2], P. Grannis[8], E. Gross[26], J. Hagemann[27], G.G. Hanson[12], M. Hansroul[8], C.K. Hargrove[7], J. Hart[8], P.A. Hart[9], M. Hauschild[8], C.M. Hawkes[8], E. Heflin[4], R.J. Hemingway[6], G. Herten[10], R.D. Heuer[8], J.C. Hill[5], S.J. Hillier[8], T. Hilse[10], D.A. Hinshaw[18], P.R. Hobson[25], D. Hochman[26], A. Höcker[3], R.J. Homer[1], A.K. Honma[28,a], R.E. Hughes-Jones[16], R. Humbert[10], P. Igo-Kemenes[11], H. Ihssen[11], D.C. Imrie[25], A. Jawahery[17], P.W. Jeffreys[20], H. Jeremie[18], M. Jimack[1], M. Jones[6], R.W.L. Jones[8], P. Jovanovic[1], C. Jui[4], D. Karlen[6], K. Kawagoe[24], T. Kawamoto[24], R.K. Keeler[28], R.G. Kellogg[17], B.W. Kennedy[20], B. King[8], J. King[13], S. Kluth[5], T. Kobayashi[24], M. Kobel[10], D.S. Koetke[8], T.P. Kokott[3], S. Komamiya[24], R. Kowalewski[8], R. Howard[29], P. Krieger[6], J. von Krogh[11], P. Kyberd[13], G.D. Lafferty[16], H. Lafoux[8], R. Lahmann[17], J. Lauber[8], J.G. Layter[4], P. Leblanc[18], P. Le Du[21], A.M. Lee[31], E. Lefebvre[18], M.H. Lehto[15], D. Lellouch[26], C. Leroy[18], J. Letts[4], L. Levinson[26], Z. Li[12], F. Liu[29], S.L. Lloyd[13], F.K. Loebinger[16], G.D. Long[17], B. Lorazo[18], M.J. Losty[7], X.C. Lou[8], J. Ludwig[10], A. Luig[10], M. Mannelli[8], S. Marcellini[2], C. Markus[3], A.J. Martin[13], J.P. Martin[18], T. Mashimo[24], P. Mättig[3], U. Maur[3], J. McKenna[29], T.J. McMahon[1], A.I. McNab[13], J.R. McNutt[25], F. Meijers[8], F.S. Merritt[9], H. Mes[7], A. Michelini[8], R.P. Middleton[20], G. Mikenberg[26], J. Mildenberger[6], D.J. Miller[15], R. Mir[26], W. Mohr[10], C. Moisan[18], A. Montanari[2], T. Mori[24], M. Morii[24], U. Müller[3], B. Nellen[3], B. Nijjhar[16], S.W. O'Neale[1], F.G. Oakham[7], F. Odorici[2], H.O. Ogren[12], C.J. Oram[28,a], M.J. Oreglia[9], S. Orito[24], J.P. Pansart[21], G.N. Patrick[20], M.J. Pearce[1], P. Pfister[10], P.D. Phillips[16], J.E. Pilcher[9], J. Pinfold[30], D. Pitman[28], D.E. Plane[8], P. Poffenberger[28], B. Poli[2], A. Posthaus[3], T.W. Pritchard[13], H. Przysiezniak[18], M.W. Redmond[8], D.L. Rees[8], D. Rigby[1], M. Rison[5], S.A. Robins[13], D. Robinson[5], J.M. Roney[28], E. Ros[8], S. Rossberg[10], A.M. Rossi[2], M. Rosvick[28], P. Routenburg[30], Y. Rozen[8], K. Runge[10], O. Runolfsson[8], D.R. Rust[12], M. Sasaki[24], C. Sbarra[2], A.D. Schaile[8], O. Schaile[10], F. Scharf[3], P. Scharff-Hansen[8], P. Schenk[4], B. Schmitt[3], H. von der Schmitt[11], M. Schröder[12], H.C. Schultz-Coulon[10], P. Schütz[3], M. Schulz[8], C. Schwick[27], J. Schwiening[3], W.G. Scott[20], M. Settles[12], T.G. Shears[5], B.C. Shen[4], C.H. Shepherd-Themistocleous[7], P. Sherwood[15], G.P. Siroli[2], A. Skillman[16], A. Skuja[17], A.M. Smith[8], T.J. Smith[28], G.A. Snow[17], R. Sobie[28], R.W. Springer[17], M. Sproston[20], A. Stahl[3], C. Stegmann[10], K. Stephens[16], J. Steuerer[28], B. Stockhausen[3], R. Ströhmer[11], D. Strom[19],

P. Szymanski[20], H. Takeda[24], T. Takeshita[24], S. Tarem[26], M. Tecchio[9], P. Teixeira-Dias[11], N. Tesch[3], M.A. Thomson[15], S. Towers[6], T. Tsukamoto[24], M.F. Turner-Watson[8], D. Van den plas[18], R. Van Kooten[12], G. Vasseur[21], M. Vincter[28], A. Wagner[27], D.L. Wagner[9], C.P. Ward[5], D.R. Ward[5], J.J. Ward[15], P.M. Watkins[1], A.T. Watson[1], N.K. Watson[7], P. Weber[6], P.S. Wells[8], N. Wermes[3], B. Wilkens[10], G.W. Wilson[4], J.A. Wilson[1], V-H. Winterer[10], T. Wlodek[26], G. Wolf[26], S. Wotton[11], T.R. Wyatt[16], A. Yeaman[13], G. Yekutieli[26], M. Yurko[18], W. Zeuner[8], G.T. Zorn[17].

[1]School of Physics and Space Research, University of Birmingham, Birmingham B15 2TT, UK
[2]Dipartimento di Fisica dell' Università di Bologna and INFN, I-40126 Bologna, Italy
[3]Physikalisches Institut, Universität Bonn, D-53115 Bonn, Germany
[4]Department of Physics, University of California, Riverside CA 92521, USA
[5]Cavendish Laboratory, Cambridge CB3 0HE, UK
[6]Carleton University, Department of Physics, Colonel By Drive, Ottawa, Ontario K1S 5B6, Canada
[7]Centre for Research in Particle Physics, Carleton University, Ottawa, Ontario K1S 5B6, Canada
[8]CERN, European Organisation for Particle Physics, CH-1211 Geneva 23, Switzerland
[9]Enrico Fermi Institute and Department of Physics, University of Chicago, Chicago IL 60637, USA
[10]Fakultät für Physik, Albert Ludwigs Universität, D-79104 Freiburg, Germany
[11]Physikalisches Institut, Universität Heidelberg, D-69120 Heidelberg, Germany
[12]Indiana University, Department of Physics, Swain Hall West 117, Bloomington IN 47405, USA
[13]Queen Mary and Westfield College, University of London, London E1 4NS, UK
[14]Birkbeck College, London WC1E 7HV, UK
[15]University College London, London WC1E 6BT, UK
[16]Department of Physics, Schuster Laboratory, The University, Manchester M13 9PL, UK
[17]Department of Physics, University of Maryland, College Park, MD 20742, USA
[18]Laboratoire de Physique Nucléaire, Université de Montréal, Montréal, Quebec H3C 3J7, Canada
[19]University of Oregon, Department of Physics, Eugene OR 97403, USA
[20]Rutherford Appleton Laboratory, Chilton, Didcot, Oxfordshire OX11 0QX, UK
[21]CEA, DAPNIA/SPP, CE-Saclay, F-91191 Gif-sur-Yvette, France
[22]Department of Physics, Technion-Israel Institute of Technology, Haifa 32000, Israel
[23]Department of Physics and Astronomy, Tel Aviv University, Tel Aviv 69978, Israel
[24]International Centre for Elementary Particle Physics and Department of Physics, University of Tokyo, Tokyo 113, and Kobe University, Kobe 657, Japan
[25]Brunel University, Uxbridge, Middlesex UB8 3PH, UK
[26]Particle Physics Department, Weizmann Institute of Science, Rehovot 76100, Israel
[27]Universität Hamburg/DESY, II Institut für Experimental Physik, Notkestrasse 85, D-22607 Hamburg, Germany
[28]University of Victoria, Department of Physics, P O Box 3055, Victoria BC V8W 3P6, Canada
[29]University of British Columbia, Department of Physics, Vancouver BC V6T 1Z1, Canada
[30]University of Alberta, Department of Physics, Edmonton AB T6G 2J1, Canada
[31]Duke University, Dept of Physics, Durham, NC 27708-0305, USA

[32]Technische Hochschule Aachen, III Physikalisches Institut, Sommerfeldstrasse 26-28, D-52056 Aachen, Germany

[a]Also at TRIUMF, Vancouver, Canada V6T 2A3

1 Introduction

Within the Standard Model, the theory of the strong interactions, Quantum Chromo Dynamics (QCD), depends on the colour charge of the quarks but is assumed to be independent of the flavour quantum number of the participating quarks [1]. Thus a precise measurement of the strong coupling constant, α_s, for a given flavour and a comparison with the value obtained by averaging over all flavours constitute an important test of the theory.

One of the most precise determinations of α_s for the inclusive case has been made in studies of gluon bremsstrahlung in hadronic decays at LEP [2]. The uncertainty in the value of $\alpha_s(M_Z)$ is about 5%, the precision being limited mainly by theoretical uncertainties associated with higher order effects. A similar precision was obtained for α_s from a fit to the hadronic width of the Z at LEP [3].

Measurements regarding the flavour dependence of α_s have also been made at LEP [4][5][6]. A comprehensive investigation was made in a previous OPAL study [5], where the differential two-jet rates and the corresponding values of α_s were measured for all five flavours. In that study the most precise result was obtained for the bottom flavour, with an uncertainty of about 3% for the ratio $\alpha_s^{\mathrm{b}}/\alpha_s^{\mathrm{incl}}$. In that analysis semi-leptonic decays were used to separate b events from those due to other flavours. The result was mainly limited by the systematic error due to our understanding of the momentum and transverse momentum spectra of the lepton.

In the present paper we report on an improved measurement of event shape distributions for $Z^0 \to b\bar{b}$ events relative to those for all flavours. Events due to b quarks are identified using secondary vertex information. Hadrons containing b quarks can decay weakly, giving rise to detectable decay lengths of order 1 - 2 mm, at LEP energies. In the following, such weak decays are referred to as b hadron decays. The secondary vertex decay length distribution is used to extract the event shape distributions for b quarks, and these distributions are in turn used to extract the ratio $\alpha_s^{\mathrm{b}}/\alpha_s^{\mathrm{incl}}$. Both the statistical and the systematic errors can be reduced significantly compared with our previous analysis.

QCD calculations of event shape variables for the process $Z^0 \to q\bar{q}g$ for massive quarks exist only in $\mathcal{O}(\alpha_s)$ [7][8]. The calculation by Ballestrero *et al.* [7] includes quark polarisation effects due to the electroweak coupling of the quarks to the Z^0, whereas that of Ioffe [8] is only for the electromagnetic case. For this reason we compare our measurements to the calculation of [7]. We estimate the mass dependence of higher orders from parton shower calculations as given in JETSET[9], HERWIG [10], and ARIADNE[11] . By applying the analysis to seven different event shape observables we check for consistency among the results obtained.

The structure of the paper is as follows. In section 2, a brief description of the OPAL detector and of the data selection is presented. The separation of b quarks from the other flavours and the measurement of the event shape distributions at the detector level are described in section 3. In section 4 the distributions are corrected for detector and fragmentation effects and then compared with massive $\mathcal{O}(\alpha_s)$ and parton shower predictions. In section 5 we discuss the contributions of higher order effects and the determination of $\alpha_s^{\rm b}/\alpha_s^{\rm incl}$.

2 The OPAL Detector and Hadronic Event Selection

The OPAL detector has been described in detail elsewhere [12]; only a brief account of some relevant features and of the selection of hadronic Z^0 decays is given here. Of particular importance to this analysis are the central drift chambers, the electromagnetic calorimeter, and the silicon microvertex detector.

The tracking of charged particles is performed with the central tracking system, composed of three systems of drift chambers: an inner vertex chamber, a large volume jet chamber and specialized chambers at the outside radius of the jet chamber which improve measurements in the z-direction. Our coordinate system is defined so that z is the coordinate parallel to the beam axis, r is the coordinate normal to the beam axis, ϕ is the azimuthal angle and θ is the polar angle with respect to z. The tracking detector is enclosed by a solenoidal magnet coil providing an axial field of approximately 0.435T. The main tracking detector for the present analysis is the jet chamber, which provides up to 159 space-points and close to 100% track finding efficiency for charged tracks in the region $|\cos\theta| < 0.92$. The momentum resolution for charged tracks is $\Delta p_{r\phi}/p_{r\phi} = \sqrt{(0.020)^2 + (0.0015 \cdot p_{r\phi})^2}$, where $p_{r\phi}$ is the transverse momentum in the $r\phi$ plane measured in GeV/c, and the average angular resolution is about 0.1 mrad in ϕ and typically 10 mrad in θ.

Electromagnetic energy is measured by a calorimeter consisting of 11704 lead-glass blocks. Each block has approximately 40×40 mrad^2 cross section, and the total range in polar angle covered is $|\cos\theta| < 0.98$, with a total solid angle coverage of 98% of 4π. The depth of the lead glass blocks is about 25 radiation lengths, and typically 2 hadronic absorption lengths. Thus, essentially all electromagnetic energy is detected in the lead glass, together with a significant fraction of hadronic energy. The basic entities used in the present analyses are clusters of energy, i.e. groups of contiguous blocks containing a non-negligible amount of energy. In order to minimize double counting of energy, clusters are accepted only if they are unassociated with a charged track. A cluster is considered to be associated with a charged track if the extrapolated track coordinates at the entrance of the calorimeter match to better than 80 mrad in ϕ and 150 mrad in θ, if the cluster is in the barrel, or 50 mrad in both ϕ and θ, if it is in the endcap.

Of particular importance to this analysis is the silicon microvertex detector [13], installed during the 1990-1991 LEP shutdown. This device consists of two layers of silicon microstrip detectors, read out in r-ϕ only, positioned close to the e^+e^- collision point, one at a radius of 6.1 cm with an angular coverage of $|\cos\theta| < 0.83$ and one at a radius of 7.5 cm with a coverage of $|\cos\theta| < 0.77$. For the data sample analysed, we achieve an effective r-ϕ positional resolution of about 10 μm with this detector and an efficiency of about 95% for finding at least one silicon

detector hit on a track, for tracks in multihadronic events which are reconstructed in the other tracking chambers and which pass through the active silicon region.

The OPAL trigger system is described in [14] and the selection procedures for hadronic events are discussed in [15]. Within the geometrical region used for the present study the efficiency of this selection is greater than 99.6%. The tracks and neutral clusters used in this analysis were subjected to quality cuts. Charged tracks were required to have at least 40 measured points in the central jet chamber, to have a transverse momentum $p_{r\phi}$ greater than 0.15 GeV/c, and to point to the origin to within 5 cm in the $r\phi$ plane and to within 25 cm in the z direction. Events containing tracks with a measured momentum greater than 60 GeV/c were rejected. Neutral clusters were required to have an energy greater than 0.2 GeV and to consist of at least two lead glass blocks. In order to compute particle energies the pion hypothesis was made for charged particles and the photon hypothesis for neutral clusters.

We imposed additional event cuts to eliminate residual background and to provide a data sample of good quality. The essential detectors (the central jet chamber, electromagnetic calorimeters and the silicon vertex detector) were required to be fully operational. The thrust axis of the event was calculated using charged tracks and clusters of electromagnetic energy, and was required to satisfy $|\cos(\theta_{\rm thrust})| < 0.7$, in order to have most tracks in the acceptance of the silicon vertex detector. The number of well measured tracks was required to be at least 9, after which the number of $\tau^+\tau^-$ and two-photon events was negligible. The multiplicity requirement was made in order to obtain events with a sufficient number of tracks to study well the transition from two to three jet events. After these cuts, approximately 550,000 events taken in 1991 and 1992 remain for analysis.

3 The separation of b from udsc quarks

3.1 The vertex tag

Since the track resolution is significantly better in the $r\phi$-plane than in the z-direction, the reconstruction of vertices was done exclusively in the $r\phi$-plane. The primary vertex for each event was reconstructed using a χ^2 minimization method which also incorporates the average beam spot position as a constraint in the vertex fit[16]. In order to find secondary vertices, the tracks and clusters were first combined into jets. This was done with the JADE jet algorithm and recombination scheme [17] and a cutoff on the minimum pair mass squared of 49 $(\mathrm{GeV}/c^2)^2$. The jet finding was carried out using the charged tracks and unassociated neutral clusters defined in section 2. The average number of jets per event was found to be 3.3. The tracks used for the reconstruction of a secondary vertex had to satisfy additional selection criteria. The impact parameter d_0 relative to the primary vertex had to satisfy $|d_0| < 0.3\,\mathrm{cm}$ and its error $\sigma_{d_0} < 0.1\,\mathrm{cm}$. This mainly removes poorly measured tracks and tracks from K^0 or Λ^0 decays. Furthermore, a minimum track momentum of 0.5 GeV/c was required.

The secondary vertex was then obtained in the following way. In a first iteration, all the charged tracks in a given jet were fitted to a common vertex point. If any charged track contributed $\Delta\chi^2 > 4$ to the overall χ^2 for the secondary vertex fit, then the track with the

largest $\Delta\chi^2$ was removed and the fit repeated. This process was continued until all tracks contributed $\Delta\chi^2 < 4$ or until an insufficient number of charged tracks remained, in which case the secondary vertex reconstruction failed for this particular jet. For this analysis, a secondary vertex was required to contain at least four associated charged tracks. Furthermore at least two of these tracks had to deviate significantly from the primary vertex by requiring that $d/\sigma_d > 2.5$, where d is the track's signed impact parameter [18] relative to the primary vertex and σ_d is the computed measurement error. With this algorithm a decay vertex will typically be reconstructed if the number of tracks from the decay of the b hadron is larger than the number of tracks in the jet originating from the primary vertex. Although the decay length distribution for charmed hadrons like the $D^{\pm}$ is similar to that for b hadrons, this algorithm reconstructs secondary vertices with high efficiency only for b hadrons. This is because the mean number of reconstructed charged tracks is significantly larger for b decays (5.4 for b hadron decays and 2.9 for c hadron decays in JETSET, as compared with four required tracks from the secondary vertex).

For each reconstructed secondary vertex, the projected decay length L was defined as the distance of the secondary vertex from the primary vertex, constrained by the direction given by the total momentum vector (in the plane transverse to the beam direction). This total momentum vector was also used to determine the sign of the decay length: $L > 0$ if the secondary vertex was displaced from the primary vertex in the same direction as the total momentum, and $L < 0$ otherwise. The ratio L/σ, where σ is the computed error on the decay length L, was used in the following analysis to discriminate between b events and u,d,s and c events. If a jet contained a secondary vertex with a value of L/σ in the range $(L/\sigma)^{\min} < L/\sigma < (L/\sigma)^{\max}$, the jet was considered to have a vertex tag. Central values $(L/\sigma)^{\min} = 1.0$ and $(L/\sigma)^{\max} = 40.0$ were chosen for this analysis.

The L/σ distribution is shown in fig. 1, both for positive and negative values. Also shown in fig. 1 are the predictions of JETSET, with full detector simulation[19]. For JETSET a b lifetime of 1.5 ps was assumed and the charged multiplicity in b hadron decays, as measured in the detector, was increased by 10%, as compared to that obtained with the standard parameters, consistent with the measurements of reference [18]. The distribution at negative values of L/σ is mainly determined by the detector resolution. As discussed in [18], the decay length resolution predicted by the detector simulation is significantly better than that in the data. This was taken into account by applying additional smearing to the Monte Carlo, involving a single parameter β. The difference between the parameters d_0, ϕ_0, and κ of the reconstructed tracks and of their associated generated particles was multiplied by a factor β, where d_0 is the distance of closest approach to the primary vertex in the $r\phi$ plane, ϕ_0 the azimuthal angle of the tangent to the track at the point of closest approach, and κ the curvature of the track. Studies of the decay length L/σ for negative values [20] and similar studies of other lifetime distributions [18][21] indicate that the detector resolution can be best described with a global smearing of the resolution by a factor of 1.2 to 1.4. In fig. 1, the JETSET predictions are shown for both these values. This range covers the data, in the region of negative values of L/σ, and is used to assess the systematic error due to uncertainties in the detector resolution. For the central analysis we took the average of the results obtained with these two smearing factors. For positive values of L/σ, the slope of the simulation is slightly different from that of the data. This will be taken into consideration by a variation of the b lifetime and b multiplicity used in the simulation and will be discussed in section 4.2.

Also given in fig. 1 is the relative contribution of the background from udsc events. For $L/\sigma > 1.0$ the fraction of b events is 89%, rising to 94% for $L/\sigma > 5.0$. The corresponding efficiencies are 26% and 22%.

3.2 Event shape variables

In first order, $\mathcal{O}(\alpha_s)$, and for massless partons, all event shape variables discussed in this paper, except the energy-energy correlation, are equivalent to each other. This changes, even in first order, if mass effects are included and is generally not true if higher orders are taken into account. To be sensitive to both these effects, we analysed seven different variables:

Differential jet rates: We used the JADE jet finder [17] and two different recombination schemes, JADE and P0 [22], to define jets. In order to have a distribution in which the bins are not statistically correlated the differential $D_2(y)$ distribution was analyzed.

$$D_2(y) = \frac{R_2(y) - R_2(y - \Delta y)}{\Delta y}, \tag{1}$$

where $R_2(y)$ is the fraction of two-jet events for a given jet resolution parameter y and Δy is the bin size. $D_2(y)$ measures the distribution of the y values for which the jet multiplicity of the events changes from three to two [22]. Each hadronic event contributes exactly once to this distribution.

Thrust: The thrust T is defined [23] by

$$T = max \left(\frac{\sum_a |\vec{p}_a \cdot \hat{n}|}{\sum_a |\vec{p}_a|} \right); \tag{2}$$

where a runs over all the final state particles, and the axis $\hat{n}$ is chosen to maximize the value of T.

Jet masses: These variables have been proposed in [24]. The particles in each event are divided into two groups by a plane orthogonal to the thrust axis, and their invariant masses are computed. We denote the heavier mass by M_H and the lighter mass by M_L. In the analysis we consider three mass variables:

M_H^2/E_{vis}^2, the heavy jet mass,

$M_D^2/E_{vis}^2 = M_H^2/E_{vis}^2 - M_L^2/E_{vis}^2$, the difference of jet masses,

M_J^2/E_{vis}^2, both the heavy and the light jet mass, with two entries per event,

where E_{vis} is the visible energy, i.e., the sum of the energies of all tracks and unassociated clusters used in the event.

Energy-energy correlation: The energy-energy correlation function Σ_{EEC} [25] is defined in terms of the angle χ_{ij} between two particles i and j of an event:

$$\Sigma_{EEC}(\chi) = \frac{1}{\Delta\chi \cdot N_{events}} \sum_{\text{events}} \int_{\chi-\Delta\chi/2}^{\chi+\Delta\chi/2} \sum_{i,j} \frac{E_i E_j}{E_{vis}^2} \cdot \delta(\chi' - \chi_{ij})\, d\chi' , \qquad (3)$$

where E_i and E_j are the energies of particles i and j and $\Delta\chi$ is the angular bin width. The normalization is such that the integral of $\Sigma_{EEC}(\chi)$ from $\chi = 0°$ to $180°$ equals unity.

The correlation between the vertex tag and the shape variables is reduced by searching for secondary vertices only in the hemisphere with the smaller invariant mass, for all variables except M_J^2/E_{vis}^2 [20]. For the variable M_J^2/E_{vis}^2, where both hemispheres are used independently, the correlation is reduced by searching for a secondary vertex only in the hemisphere opposite to that used for the calculation of M_J^2/E_{vis}^2. A small residual bias on the event shape distributions due to the vertex tag remains, as illustrated in Fig. 2a for example, for the case of the differential jet rate using the JADE recombination scheme. The figure shows the ratio of the distributions, $D_2^{\text{b, vertex tag}}/D_2^{\text{b, all}}$, as obtained from JETSET, for all b events and those b events satisfying the vertex tag $1.0 < L/\sigma < 9.0$. The ratio for a more severe tag, $9.0 < L/\sigma < 40.0$, is given as well. For y values smaller than 0.1, the deviation of the ratio from unity is less than or of order 10%. The bias for the vertex tag used for the main analysis can be obtained from the figure by averaging the two results shown. For y values larger than 0.1 the efficiency of the tag decreases. The variation of the tagging efficiency with y was studied with JETSET. It was found that the average b momentum decreases with increasing y and that the vertex tag becomes less efficient for smaller b momenta. For the other shape variables studied except the energy-energy correlation, the biases are very similar to that of $D_2(y)$, both in magnitude and shape, and are not shown. The bias introduced for the energy-energy correlation is shown in Fig. 2b. The bias is significantly smaller than for the other variables, less than 5% for all y values. Note that the bias is fully taken into account in the maximum likelihood analysis discussed in the following section. The potential systematic error produced will be estimated by a variation of the lifetime and decay multiplicity of b hadrons, the hardness of the fragmentation function, etc., as discussed in section 4.2.

3.3 Likelihood fit

The aim of the following analysis is to determine the distributions of the seven variables defined in section 3.2, for b quarks. In order to use the full information of all events, this was done using an event by event likelihood fit, which we now describe.

The distributions of the observables are denoted by the function $F(\tilde{y}) = dN/d\tilde{y}$, where $\tilde{y}$ stands for one of the observables. For the differential jet rate, for example, $F(\tilde{y}) = D_2(y)$, with $\tilde{y} = y$. For the likelihood fit the distribution $F(\tilde{y})$ was divided into eight $\tilde{y}$ bins and the flavour separation was done separately for each of these bins. The analysis is based on the electroweak couplings of the Standard Model, as well as on JETSET with full detector simulation, from which the efficiencies and the density functions in L/σ were taken. This will be discussed in detail below. The result of the likelihood fit is the measured ratio of the distributions for b quarks to those for all quarks, $R_i^{\text{b}} = F^{\text{b}}(\tilde{y}_i)/F^{\text{incl}}(\tilde{y}_i)$ where i=1 to 8 denotes the i'th $\tilde{y}$ bin. This

is achieved by making separate fits for each of the eight $\tilde{y}$ bins with $R_i^{\rm b}$ as the free parameter. As will be shown the bias introduced by the tag procedure is automatically taken into account in the likelihood analysis.

In the likelihood fit, all events, with and without a secondary vertex tag (defined by $(L/\sigma)^{\rm min} < L/\sigma < (L/\sigma)^{\rm max}$, as discussed in section 3.1) are used. When fitting the i'th $\tilde{y}$-bin, we take into account the contributions from the events in bin i as well as the contributions from those events falling into the other bins. This guarantees that the total number of events of a certain flavour will be equal to the expected number of events, which is taken from JETSET with the Standard Model electroweak couplings. Furthermore, one becomes insensitive to systematic effects contributing equally to all $\tilde{y}$-bins. An overall likelihood $\mathcal{L}^i$ for all events is thus calculated:

$$\mathcal{L}^i = \prod_{j=1}^{8} \prod_{\rm events} \mathcal{L}_j^i. \tag{4}$$

Here $\mathcal{L}_j^i$ is the likelihood for an event in bin j, when fitting bin i. The likelihood depends on whether the event has a vertex tag and, if it has a vertex tag, is a function of L/σ.

The likelihood is given by

$$\mathcal{L}_j^i = \begin{cases} \sum\limits_{f={\rm b,udsc}} \eta_{ij}^f \frac{N_j^{f,{\rm vertex}}}{N_j^f} \hat{\rho}_j^f(L/\sigma) & \text{vertex tag, i.e.} \quad L/\sigma \in \left[(L/\sigma)^{\rm min}, (L/\sigma)^{\rm max}\right] \\ \sum\limits_{f={\rm b,udsc}} \eta_{ij}^f (1 - \frac{N_j^{f,{\rm vertex}}}{N_j^f}) & \text{no vertex tag} \end{cases} \tag{5}$$

If an event lies in bin $j = i$, the quantity $\eta_{i,j=i}^f$ is defined as N_i^f/N_i, the unknown ratio of the number of events with flavour f in bin i over the total number of events in bin i. $N_i^{f,{\rm vertex}}/N_i^f$ is the relative fraction of events of flavour f with a secondary vertex tag in bin i, and $\hat{\rho}_i^f(L/\sigma)$ is the probability density function of L/σ within the vertex tag range, for flavour f. It is normalized as follows: $\int_{(L/\sigma)^{\rm min}}^{(L/\sigma)^{\rm max}} \hat{\rho}_i^f(L/\sigma)\, d(L/\sigma) = 1$. The values for $\hat{\rho}_i^f(L/\sigma)$ and $N_i^{f,{\rm vertex}}/N_i^f$ were taken from JETSET with full detector simulation [19]. By allowing these quantities to depend on the bin number, i, we are taking into account the bias introduced by the tag procedure as noted in the discussion of fig. 2 (section 3.2). If an event lies in bin $j \neq i$, the quantity $\eta_{i,j\neq i}^f$ is defined as $\sum_{k\neq i} N_k^f / \sum_{k\neq i} N_k$, the unknown fraction of the events with flavour f for all bins other than bin i. The unknown fractions η_{ij}^f can be expressed using the ratio

$$R_i^f \equiv \frac{N_i^f}{N^f} \Big/ \frac{N_i}{N}, \qquad f = {\rm b, udsc} \tag{6}$$

as

$$\eta_{i,j=i}^f \equiv \frac{N_i^f}{N_i} = R_i^f \frac{N^f}{N} \qquad \text{and} \qquad \eta_{i,j\neq i}^f \equiv \frac{\sum_{k\neq i} N_k^f}{\sum_{k\neq i} N_k} = \frac{N^f - N_i^f}{N - N_i} = \frac{1 - R_i^f \frac{N_i}{N}}{1 - \frac{N_i}{N}} \frac{N^f}{N}, \tag{7}$$

where N^f is the number of events with flavour f = b or udsc, and N the total number of events. The quantity N^f/N is given by the electroweak couplings and by detector and selection efficiencies, N_i/N is known from the data, and $R_i^{\rm udsc}$ may be expressed as $R_i^{\rm udsc} =$

$(1 - R_i^{\rm b} N^{\rm b}/N)/(1 - N^{\rm b}/N)$. Therefore the likelihood can be maximized with $R_i^{\rm b}$ as the only free parameter. In terms of the distribution, $F(\tilde{y})$, $R_i^{\rm b}$ is just the ratio of the normalized $F(\tilde{y})$ distribution for b events, to the normalized $F(\tilde{y})$ distribution for all events,

$$R_i^{\rm b} \equiv R^{\rm b}(\tilde{y}_i) = \frac{F^{\rm b}(\tilde{y}_i)}{F^{\rm incl}(\tilde{y}_i)}. \tag{8}$$

All variables analysed except the energy-energy correlation are of the form $dN/d\tilde{y}$ and contribute one entry per event to the distribution, while the variable M_J^2/E_{vis}^2 contributes one entry per hemisphere. For these variables the function $F(\tilde{y})$ is given by

$$F(\tilde{y}) = \begin{cases} D_2(y) \\ dN/d(1-T) \\ dN/d(M_x^2/E_{vis}^2) \quad x = H, D, J \end{cases} \qquad \tilde{y} = \begin{cases} y \\ 1-T \\ M_x^2/E_{vis}^2 \quad x = H, D, J \end{cases} . \tag{9}$$

In order to use the above ansatz also for the energy-energy correlation, which is not of the form $dN/d\tilde{y}$, the following special procedure was adopted. The $\Sigma_{EEC}(\chi)$ distribution was divided into 12 equal bins of χ. The contribution of each event to the k'th χ-bin is given by:

$$\Sigma_{EEC}^k = \frac{1}{\Delta\chi} \int_{\chi_k^{\rm min}}^{\chi_k^{\rm max}} \sum_{i,j} \frac{E_i E_j}{E_{vis}^2} \cdot \delta(\chi' - \chi_{ij})\, d\chi' , \tag{10}$$

where $\chi_k^{\rm min} = (k-1) \cdot \Delta\chi$ and $\chi_k^{\rm max} = k \cdot \Delta\chi$ define the k'th bin and $\Delta\chi = 15°$. Each event has one contribution Σ_{EEC}^k to the k'th bin, which is, in general, different from event to event. Thus one obtains 12 distributions $F^k(\Sigma_{EEC}^k) = dN/d\Sigma_{EEC}^k$, for $k = 1, ..., 12$, of the form $dN/d\tilde{y}$ as required for the likelihood method. The distribution $dN/d\Sigma_{EEC}^k$ for b quarks is now determined in a likelihood fit for eight Σ_{EEC}^k bins, separately for each of the 12 χ-bins. The energy-energy correlation, for the k'th bin, is then given by the average (see equ. (3))

$$\Sigma_{EEC}(\chi = \chi^k) = \frac{1}{N_{events}} \sum_{\rm events} \Sigma_{EEC}^k = \left\langle \Sigma_{EEC}^k \right\rangle , \tag{11}$$

where χ^k is the centre of the k'th χ bin. Since the distributions are binned, the average is computed in the following way. The quantity $dN/d\Sigma_{EEC}^k$, for a given χ bin, is multiplied by the mean value of Σ_{EEC}^k in that bin, and then the sum is taken over the eight Σ_{EEC}^k bins. This mean value of Σ_{EEC}^k for one bin is not known, a priori, for b quarks. It is taken from the data, i.e. for all flavours, and then corrected for b quarks using JETSET information.

4 Results

4.1 Detector and fragmentation correction

For each event shape variable $F(\tilde{y})$, the result of the likelihood analysis discussed in section 3.3 is the function $R^{\rm b}(\tilde{y})$, the ratio of the normalized $F(\tilde{y})$ distributions for b events to those for all events, at the detector level. In order to compare the results with the massive $\mathcal{O}(\alpha_s)$ calculation,

we correct them to the *particle* level for effects of selection cuts and detector smearing, and to the *parton* level, for initial state radiation and hadronisation effects. The corrections for both these effects are carried out bin by bin, using correction factors obtained from JETSET. In this context, the particle level includes all particles except neutrinos after the decay of short-lived particles ($\tau < 3 \cdot 10^{-10} s$). The parton level is defined by the cut-off of the QCD shower in JETSET, set to $Q_0 = 1$ GeV/c^2. The correction from detector to particle level is less than, or of the order of, one per cent, for all variables. The correction to parton level is discussed in more detail in section 4.3.

The results at the particle level are given in table 1, for the ratio of the distributions of all seven event shape variables for b quarks relative to those for all quarks. The errors in table 1 include the systematic errors, which will be discussed in detail in the next section. Furthermore, the systematic error is split into an uncorrelated and a correlated contribution.

4.2 Systematic uncertainties

There are several places where systematic uncertainties enter the analysis. Various effects can influence the normalized density distributions used in the likelihood fit, as well as the correction due to detector resolution and the correction from particle level to parton level. The estimation of these systematic uncertainties follows closely the methods used in previous OPAL studies [18][26].

The following sources of systematic error were considered when determining the normalized density distributions $\hat{\rho}_i(L/\sigma)$ and $N_i^{f,\mathrm{vertex}}/N_i^f$ as a function of the bin number i.

Lifetime and Particle Composition: The results were obtained using a mean lifetime for b hadrons of 1.5 ps. This was varied, by reweighting the JETSET events, in the range from 1.4 ps to 1.6 ps, corresponding to the lifetime measurements of [21] . Furthermore the individual lifetimes of charm hadrons D^0, $\mathrm{D}^{\pm}$, D_s, and Λ_c were varied by the errors as given by the Particle Data Group [27]. In addition, the relative production rates of these hadrons were changed by varying the fraction of D^0 by 50%, and of D_s and Λ_c by 100% each.

B and D decay multiplicity: As discussed in section 3.1, the vertex tag probability depends on the charged particle multiplicity in the decay. In order to obtain a satisfactory description of the L/σ distribution by JETSET, the charged multiplicity of b hadrons, as measured in the detector, had to be increased by 10% as compared to that obtained with the standard parameters. For the systematic error the charged multiplicities for b and c hadrons were varied by an additional $\pm 10\%$.

Vertex tag efficiency: A comparison between data and simulation of the number of events with two secondary vertices[20] leads to the conclusion that the efficiency to find vertices in b events is underestimated in the simulation by about 5%. For the systematic error this efficiency was increased by 10%.

Fragmentation function: We used the Peterson *et al.* fragmentation function[28] for heavy quarks with $\epsilon_b = 0.0057$ and $\epsilon_c = 0.046$. We varied ϵ_b in the range $0.0025 \leq \epsilon_b \leq 0.0095$.

This corresponds to $< x_E > = 0.70 \pm 0.02$, where $< x_E >$ is the mean energy of hadrons containing b quarks, scaled to the center of mass energy. The range more than covers the OPAL measurement[29] of $< x_E > = 0.697 \pm 0.013$, where the error includes a variation of the shape of the fragmentation function. Note that the use of HERWIG[10] and the LUND symmetric fragmentation function[9] are not appropriate in this case since these are known not to describe the distributions for b events.

Partial widths $\Gamma_{b\bar{b}}$ and $\Gamma_{c\bar{c}}$: The main results were obtained with values of $\Gamma_{b\bar{b}}/\Gamma_{had} = 0.216$ and $\Gamma_{c\bar{c}}/\Gamma_{had} = 0.171$. These values were varied by $\pm 2\%$ for $\Gamma_{b\bar{b}}$, consistent with our measurement of $\Gamma_{b\bar{b}}$[30], and by $\pm 15\%$ for $\Gamma_{c\bar{c}}$, based on an update of the measurement in [31].

L/σ range for vertex tag : For the main analysis, secondary vertices with $L/\sigma \in \left[(L/\sigma)^{\min}, (L/\sigma)^{\max}\right]$ were considered, with $(L/\sigma)^{\min} = 1.0$ and $(L/\sigma)^{\max} = 40.0$. The lower limit was varied in the range $0 \leq (L/\sigma)^{\min} \leq 5$ and the upper limit in the range $30 \leq (L/\sigma)^{\max} \leq \infty$.

Monte Carlo statistics: The density functions $\hat{\rho}$ were determined from JETSET events with full detector simulation. The limited number of such events satisfying the vertex tag requirement introduces a significant statistical error. This error was estimated in the following way. The L/σ distribution was divided into 100 bins. Each Monte Carlo event in bin k was then reweighted with one and the same number which was chosen randomly from a Gaussian distribution with central value one and width $1/\sqrt{N_k}$, where N_k is the number of events in bin k. This procedure was repeated 100 times. The error was then estimated as the width of the resulting values for R_i^{b}.

Special procedure for the Σ_{EEC}-variable: When calculating the energy-energy correlation for the k'th bin, an average is taken over eight Σ_{EEC}^k bins, as was discussed in detail in section 3.3. The mean value of Σ_{EEC}^k for each bin, necessary for this averaging, was taken from the data and then corrected for b events, using JETSET. The systematic error of this procedure was conservatively estimated by repeating the analysis without the latter correction.

Tracking resolution: As discussed in section 3.1, the resolution of the central tracking system is not described adequately in our detector simulation. This was taken into account with a global smearing of the resolution by a factor of 1.2 to 1.4. For the systematic error the smearing factor was varied between 1.2 and 1.4. For the main analysis we took the average of the results obtained with the two values.

Detector correction: The uncertainty in the correction for detector effects was estimated by repeating the complete analysis using only the information from charged tracks (i.e. omitting the neutral clusters). The difference obtained was taken as the systematic error.

The correction from particle level to parton level gives rise to a systematic error due to uncertainties in the b fragmentation function and ambiguities in the definition of the parton level. It was estimated within JETSET in the following way:

Fragmentation function: We varied the parameter in the Peterson fragmentation function in the range $0.0025 \leq \epsilon_b \leq 0.0095$.

Termination of the parton shower: The parameter Q_0, determining the termination of the parton shower in JETSET, and thus defining the parton level, was taken as $Q_0 = 1$ GeV/c^2. It was varied in the range 1 GeV/$c^2 \leq Q_0 \leq 6$ GeV/c^2.

The variation of the b fragmentation function enters in the systematics in two places and those contributions were added linearly. The total systematic errors were then calculated by summing the individual errors in quadrature. Since in general, the systematic errors for the different $\tilde{y}$ bins are strongly correlated, they were split into two contributions. In order to calculate these we computed the mean value of the seven shape variables, averaged over the range in $\tilde{y}$ used for the α_s determination (given in table 4). The correlated error is given by how much the mean is systematically shifted in a given direction by the effects investigated. The uncorrelated error was then calculated as the difference between the total systematic error, for a given $\tilde{y}$ bin, and the correlated error. Both errors are given in table 1. A summary of all systematic errors for the mean values is given in table 2. For most variables, the major systematic contributions arise from uncertainties in the vertex efficiency, the detector correction, the b fragmentation function, and Monte Carlo statistics.

4.3 The b-quark event shape distributions

In fig. 3 a - g, the ratio of the event shape distributions for b quark events to those for all events, corrected to the parton level, is presented for all seven variables. The distributions will be compared with an $\mathcal{O}(\alpha_s)$ matrix element calculation as well as with parton shower predictions. As an example of the latter we show the JETSET predictions. In fig. 3 a - f, the first bin does not contain independent information and its value is given by the fact that both the numerator and denominator of the ratio are normalized to unity.

The data are first compared with the massive $\mathcal{O}(\alpha_s)$ calculation of [7]. The published calculation contains the second order only at tree level and includes quark polarisation effects due to the electroweak coupling of the quarks to the Z^0. Since the virtual contributions in second order, which are important for the differential three-jet-rate, are not included, we used only the $\mathcal{O}(\alpha_s)$ part of the matrix element given in the Monte Carlo generator provided by the authors. In the calculation, the b quark mass was assumed to be $m_b = 5$ GeV/c^2 and the strong coupling constant was assumed to be universal for all flavours. Also, in figure 3, the data are compared with the JETSET predictions at the parton level, as well as at the detector level. A comparison of the latter two indicates the magnitude of the correction due to detector and fragmentation. A comparison of the massive $\mathcal{O}(\alpha_s)$ calculation with the parton shower prediction is interesting as well. The $\mathcal{O}(\alpha_s)$ calculation takes into account the explicit b mass dependence of gluon radiation from b quarks. For the parton shower prediction, which is based on the leading log approximation (LLA), explicit mass terms in the Altarelli-Parisi formalism for parton radiation are missing. On the other hand, phase space effects due to the finite quark masses, which lead to an earlier termination of the shower for b quarks, are included.

Comparing the model curves at parton and detector level, one sees that the fragmentation and detector corrections are small for most variables. The corrections are large in the highest bin for the mass variables, as well as in the highest and lowest bin for the energy-energy correlation. The corrections for this variable are dominated by the correction for the b decay. These bins

will not be used for the fit of α_s, however. The only variable with fairly large corrections over the full fit range is $(1-T)$.

The data tend to lie below unity, especially for the variables $D_2(y)$-P0, $(1-T)$ and Σ_{EEC}. This can also be seen from the mean values which are given in table 1. The theoretical predictions are, for most variables, also below unity. The massive $\mathcal{O}(\alpha_s)$ calculation and the JETSET parton shower prediction deviate significantly from each other for the variable $(1-T)$, and for the jet masses. The data are consistent with both predictions and are not precise enough to discriminate between them.

5 Determination of $\alpha_s^{\mathrm{b}}/\alpha_s^{\mathrm{incl}}$

In order to determine the ratio $\alpha_s^{\mathrm{b}}/\alpha_s^{\mathrm{incl}}$ from the event shape distributions at the parton level we first correct the data using the massive $\mathcal{O}(\alpha_s)$ calculation. The corrected ratio, $R^{\mathrm{cor}}(\tilde{y})$, is obtained from that at parton level, $R^{\mathrm{parton}}(\tilde{y})$, as

$$R^{\mathrm{cor}}(\tilde{y}) = R^{\mathrm{parton}}(\tilde{y}) \frac{1}{R_{\mathcal{O}(\alpha_s)}(\tilde{y})}, \tag{12}$$

where $R_{\mathcal{O}(\alpha_s)}(\tilde{y})$ is the ratio of $F(\tilde{y})$ for b quarks to that for all quarks, calculated from the massive $\mathcal{O}(\alpha_s)$ expression. For the correction we used a b quark mass of $m_{\mathrm{b}} = 5.0$ GeV/c^2. For the systematic error it was varied between 5.0 and 4.5 GeV/c^2[32]. We then used the second order massless calculation[33] to fit for $\alpha_s^{\mathrm{b}}/\alpha_s^{\mathrm{incl}}$:

$$F(\tilde{y};\alpha_s(\mu)) = \frac{\alpha_s(\mu)}{2\pi} A(\tilde{y}) + \left(\frac{\alpha_s(\mu)}{2\pi}\right)^2 \left[A(\tilde{y}) 2\pi b_0 \ln(\mu^2/s) + B(\tilde{y}) - 2A(\tilde{y})\right] \tag{13}$$

with

$$b_0 = \frac{33 - 2n_f}{12\pi}.$$

Here $\sqrt{s} = M_{\mathrm{Z}}$ is the centre of mass energy, $n_f = 5$ the number of flavours and μ the renormalisation scale. The strong coupling constant at a given scale μ is given by

$$\alpha_s(\mu) = \frac{1}{b_0 \ln(\mu^2/\Lambda^2)} - \frac{b_1 \ln(\ln(\mu^2/\Lambda^2))}{(b_0 \ln(\mu^2/\Lambda^2))^2}$$

with

$$b_1 = \frac{153 - 19n_f}{24\pi^2}$$

and Λ is the QCD scale parameter. For the observables $(1-T)$, M_H^2/E_{vis}^2, M_D^2/E_{vis}^2, and Σ_{EEC} the functions A$(\tilde{y})$ and B$(\tilde{y})$ were taken from [33], for $D_2(y)$-JADE and $D_2(y)$-P0 from [34]. For the new variable M_J^2/E_{vis}^2, which has not been used previously, the matrix element generator written by the authors of [33] was used to determine the functions.

One then obtains , for the ratio of the distributions for b and all quarks, the theoretical fit expression

$$R_{\mathrm{fit}}^{\mathrm{b}}(\tilde{y}) = \frac{F(\tilde{y};\alpha_s^{\mathrm{b}}(\mu))}{F(\tilde{y};\alpha_s^{\mathrm{incl}}(\mu))}. \tag{14}$$

Substituting $\alpha_s^{\rm b} = \alpha_s^{\rm incl} \times \alpha_s^{\rm b}/\alpha_s^{\rm incl}$, and keeping $\alpha_s^{\rm incl}(M_{\rm Z})$ fixed to the average determined previously[26], $\alpha_s^{\rm incl}(M_{\rm Z}) = 0.122$, the ratio $\alpha_s^{\rm b}(\mu)/\alpha_s^{\rm incl}(\mu)$ was then determined as the only free parameter. A variation of $\alpha_s^{\rm incl}(M_{\rm Z})$ in the range 0.11 - 0.13 had a negligible effect on the fit result. In the main fit we fixed the renormalisation scale $x_\mu = \mu/\sqrt{s}$ to unity and used the same scale for $\alpha_s^{\rm b}$ and $\alpha_s^{\rm incl}$. The quoted systematic error includes an additional error contribution due to a variation of that scale. It was varied between unity and the optimal scale, $x_\mu^{\rm opt}$, as obtained in an analysis of the inclusive sample [26]. For M_J^2/E_{vis}^2, which has not been studied previously, $x_\mu^{\rm opt}$ was taken to be equal to that for M_H^2/E_{vis}^2. For the Σ_{EEC} variable, the optimal scale was taken from [35]. The optimal scales used are given in table 3. In order to check the consistency of the results we performed fits over different ranges for the distributions. For all variables except the energy-energy correlation the fits were repeated in the ranges 0.050 - 0.2 and 0.065 - 0.2. For $\Sigma_{\rm EEC}$ the ranges 60° - 120° and 75° - 105° were taken. The results obtained were entirely compatible, within the statistical errors.

The results for $\alpha_s^{\rm b}/\alpha_s^{\rm incl}$, as well as the fit range used, are shown in table 4, and in fig. 4a, separately for the seven variables. Also given in the figure (the topmost point) is our previous result for $D_2(y)$-JADE from the lepton analysis [5]. A comparison with the corresponding point from the present analysis illustrates the significant improvement in precision resulting from the vertex tagging technique. As one can see from fig. 4a, the results for the seven shape variables are consistent with each other and with unity. Taking into account the correlations, the most significant difference is obtained between the results from $D_2(y)$-JADE and M_H^2/E_{vis}^2. One obtains, for these two variables, a difference of 2.3 standard deviations.

As mentioned earlier, both a correction for mass effects based on the $\mathcal{O}(\alpha_s)$ calculation and one based on LLA parton showers take account of phase space effects due to the b mass. Correcting with $\mathcal{O}(\alpha_s)$ partially takes into consideration, in addition, the explicit dependence of the process $\rm Z^0 \to b\bar{b}g$ on the b mass. On the other hand, a correction based on the parton shower approximately takes into account higher order QCD effects. In addition, a dependence of the higher orders on finite quark masses is accounted for by the mass dependence of the termination of the parton shower. Thus it equally makes sense to correct for mass effects using parton shower calculations. We have applied three different parton shower calculations: those used in JETSET, HERWIG, and ARIADNE. The mass corrections obtained from them are consistent with each other. They typically vary by about 1% for most variables, and the largest deviations are about 4%, for $(1-T)$ and M_D^2/E_{vis}^2. In order to take account of these theoretical uncertainties, we average the mass corrections from the three parton shower calculations and add, as a systematic error, the RMS value of the deviations. The results with this average mass correction are shown in fig. 4b and table 4. Again the results are consistent with each other, the most significant difference being 1.6 standard deviations between the results from $(1-T)$ and M_J^2/E_{vis}^2.

Since the application of either mass correction gives consistent results for all variables, and since there seems to be no clear theoretical preference for one or the other, we average the results. Thus we take the average of the values obtained with the two mass corrections and add, as an additional systematic error contribution, half the difference between the two results. This systematic error is referred to as "mass correction" in table 5. To a certain degree, this error takes account of uncertainties in the mass correction due to unknown higher orders. This result is shown in fig 4c and table 4. In table 5, we give a summary of the individual systematic errors for the average ratio $\alpha_s^{\rm b}/\alpha_s^{\rm incl}$.

For the overall result we average the individual results obtained from the seven observables. The procedure for this follows the one used previously in our global determination of α_s from many observables [26]. The weighted average of all seven results was taken, where each measurement was weighted with the inverse of the square of its total error as given in table 4 (last column). The statistical errors were treated as being fully correlated. The systematic deviations for all sources of uncertainties given in table 5 were then recomputed relative to the weighted average. They were added in quadrature to give the new systematic error. This leads to

$$\frac{\alpha_s^{\mathrm{b}}}{\alpha_s^{\mathrm{incl}}} = 0.994 \pm 0.005 \,^{+\,0.010}_{-\,0.012} \quad ,$$

where the errors are the statistical and systematic errors. We checked for consistency between the average result and the results from the individual observables by computing the χ^2 between the mean value and the individual measurements. Taking into account the correlations, we obtained χ^2 values of 5.0, 4.7, and 2.2, for six degrees of freedom, for the results with the mass correction based on $\mathcal{O}(\alpha_s)$, parton shower calculations, and the average of both, respectively. Because different observables are subject to differing higher order corrections, any inconsistency between their results could be an indication of higher order effects. Since the measurements from the seven observables are compatible within systematic errors, we conclude that the effects of higher orders are covered by the systematic errors assigned.

The ratio $\alpha_s^{\mathrm{b}}/\alpha_s^{\mathrm{incl}}$ is the ratio of the strong coupling constant for b quarks relative to that of all flavours. It can be converted into the ratio for b quarks relative to the complementary flavours not including the b quarks. This ratio is obtained as

$$\frac{\alpha_s^{\mathrm{b}}}{\alpha_s^{\mathrm{udsc}}} = 0.992 \pm 0.007 \,^{+\,0.013}_{-\,0.015} \quad .$$

6 Summary

We have measured the distributions of seven event shape observables for b events relative to those for all events, $F^{\mathrm{b}}(\tilde{y})/F^{\mathrm{incl}}(\tilde{y})$. QCD calculations in $\mathcal{O}(\alpha_s)$, available for massive quarks, describe the ratios well. Parton shower calculations, which include all orders within the leading log approximation, describe the data about equally well. After correction for b mass effects using both types of calculation as alternatives, $\alpha_s^{\mathrm{b}}/\alpha_s^{\mathrm{incl}}$ values were obtained from a fit of the theoretical $\mathcal{O}(\alpha_s^2)$ expression to the data. The uncertainty due to higher orders was estimated from the results obtained with both types of mass correction. The results obtained from the seven observables studied are consistent with each other. There is no indication from the data that the mass dependence of higher orders is significantly different for the observables studied.

For the final result we average the individual measurements, which leads to $\alpha_s^{\mathrm{b}}/\alpha_s^{\mathrm{udsc}} = 0.992 \pm 0.007 \,^{+\,0.013}_{-\,0.015}$. Our measurement can be compared with the result published by the L3 collaboration [4] $\alpha_s^{\mathrm{b}}/\alpha_s^{\mathrm{udsc}} = 1.00 \pm 0.05 \pm 0.06$ and that by DELPHI [6] $\alpha_s^{\mathrm{b}}/\alpha_s^{\mathrm{udsc}} = 1.00 \pm 0.04 \pm 0.03$. Both these results were obtained from three-jet rates using a lepton b tag. Our value is in agreement with these results but has significantly smaller errors. Overall, our measurement is consistent with unity with a precision of better than 2%. This result constitutes the most accurate test yet made of the flavour independence of the strong interactions. The measurement

can be used in the future to check higher order calculations for heavy quarks, which are being carried out at the present [36].

7 Acknowledgements

We thank W. Bernreuther for several interesting discussions concerning the theoretical aspects of this paper. We thank also A. Ballestrero, E. Maina, and S. Moretti for providing us with their Monte Carlo generator. It is a pleasure to thank the SL Division for the efficient operation of the LEP accelerator, the precise information on the absolute energy, and their continuing close cooperation with our experimental group. In addition to the support staff at our own institutions we are pleased to acknowledge the
Department of Energy, USA,
National Science Foundation, USA,
Texas National Research Laboratory Commission, USA,
Particle Physics and Astronomy Research Council, UK,
Natural Sciences and Engineering Research Council, Canada,
Fussefeld Foundation,
Israeli Ministry of Energy and Ministry of Science,
Minerva Gesellschaft,
Japanese Ministry of Education, Science and Culture (the Monbusho) and a grant under the Monbusho International Science Research Program,
German Israeli Bi-national Science Foundation (GIF),
Direction des Sciences de la Matière du Commissariat à l'Energie Atomique, France,
Bundesministerium für Forschung und Technologie, Germany,
National Research Council of Canada,
A.P. Sloan Foundation,
and Junta Nacional de Investigação Científica e Tecnológica, Portugal.

References

[1] H. Fritzsch, M. Gell-Mann, 16'th Int. Conf. on High Energy Physics, Chicago (1972);
H. Fritzsch, M. Gell-Mann and H. Leutwyler, Phys. Lett. **B47** (1973) 365;
D. Gross and F. Wilczek, Phys. Rev. Lett. **30** (1973) 1343;
H.D. Politzer, Phys. Rev. Lett. **30** (1973) 1346.

[2] S. Catani, rapporteur's talk, Int. Europhysics Conf. on High Energy Physics 1993, Marseille, p. 771, Editions Frontières, eds. J. Carr - M. Perrottet (1993);
M. Shapiro, rapporteur's talk, XVI Int. Symp. Lepton - Photon Interactions, Cornell (to be published).

[3] ALEPH Collab., D.Buskulic *et al.*, CERN-PPE/94-30, submitted to Z.Phys.C;
DELPHI Collab., P.Abreu *et al.*, Nucl. Phys. **B418** (1994) 403;
L3 Collab., M.Acciarri *et al.*, CERN-PPE/94-45, submitted to Z.Phys.C ;
OPAL Collab., R.Akers *et al.*, Z. Phys. **C61** (1994) 19.

[4] L3 Collaboration, B. Adeva *et al.*, Phys. Lett. **B271** (1991) 461.

[5] OPAL Collaboration, R. Akers *et al.*, Z. Phys. **C60** (1993) 397.

[6] DELPHI Collaboration, P. Abreu *et al.*, Phys. Lett. **B307** (1993) 221.

[7] A. Ballestrero, E. Maina, and S. Moretti, Phys. Lett. **B294** (1992) 425.

[8] B.L. Ioffe, Phys. Lett. **B78** (1978) 277.

[9] T. Sjöstrand, Comp. Phys. Comm. **39** (1986) 347;
T. Sjöstrand, Comp. Phys. Comm. **43** (1987) 367;
M. Bengtsson and T. Sjöstrand, Nucl. Phys. **B289** (1987) 810.

[10] G. Marchesini and B.R. Webber, Nucl. Phys. **B310** (1988) 461;
G. Marchesini *et al.*, Comp. Phys. Commun. **67** (1992) 465.

[11] U. Petterson, LU TP 88-5 (1988);
U. Petterson and L. Lönnblad, LU TP 88-15 (1988);
L. Lönnblad, LU TP 89-10 (1989).

[12] OPAL Collaboration, K. Ahmet *et al.*, Nucl. Instr. Methods **A305** (1991) 275.

[13] P.P. Allport *et al.*, Nucl. Instr. Methods, **A324** (1993) 34.

[14] OPAL Collaboration, M. Arignon *et al.*, Nucl. Instr. Methods **A313** (1992) 103.

[15] OPAL Collaboration, G. Alexander *et al.*, Z. Phys. **C52** (1991) 175.

[16] OPAL Collaboration, P.D. Acton *et al.*, Z. Phys. **C59** (1993) 183.

[17] JADE Collaboration, S.Bethke *et al.*, Phys. Lett. **B213** (1988) 235.

[18] OPAL Collaboration, R. Akers *et al.* Z. Phys. **C61** (1994) 209.

[19] J. Allison *et al.*, Comp. Phys. Comm. **47** (1987) 55;
J. Allison *et al.*, Nucl. Instr. Methods **A317** (1992) 47.

[20] R. Ströhmer, Ph.D. thesis, University of Heidelberg (1994), unpublished.

[21] OPAL Collaboration, P. D. Acton *et al.*, Phys. Lett. **B307** (1993) 247.

[22] OPAL Collaboration, M.Z. Akrawy *et al.*, Z. Phys. **C49** (1991) 375.

[23] S. Brandt *et al.*, Phys. Lett. **B12** (1964) 57;
E. Farhi, Phys. Rev. Lett. **39** (1977) 1587.

[24] T. Chandramohan and L. Clavelli, Nucl. Phys. **B184** (1981) 365.

[25] C.L. Basham *et al.*, Phys. Rev. Lett. **B41** (1978) 1585; Phys. Rev. **D17** (1978) 2298.

[26] OPAL Collaboration, P.D. Acton *et al.*, Z. Phys., **C55** (1992) 1.

[27] Particle Data Group, Phys. Rev. **45D** (1992) 1.

[28] C. Peterson, D. Schlatter, I. Schmitt, P.M. Zerwas, Phys. Rev. **D27** (1983) 105.

[29] OPAL Collaboration, R. Akers *et al.*, Z. Phys. **C60** (1993) 199.

[30] Measurement of $\Gamma(Z^0 \to b\bar{b})/\Gamma(Z^0 \to \text{hadrons})$ using a Double Tagging Method,
OPAL Collaboration, R. Akers *et al.*, CERN-PPE/94-106, to be submitted to Phys. Lett..

[31] OPAL Collaboration, G. Alexander *et al.*, Phys. Lett. **B262** (1991) 341.

[32] J. Gasser and H. Leutwyler, Phys. Reports, **87** (1982) 77;
S. Narison, CERN-TH/7277-94.

[33] Z. Kunszt, P. Nason in Z^0 Physics at LEP 1, G. Altarelli, R. Kleiss, C. Verzegnassi (eds.), Vol.1 CERN 89-08 (1989).

[34] S. Bethke *et al.*, Nucl. Phys. **B370** (1992) 310.

[35] OPAL Collaboration, M.Z. Akrawy *et al.*, Phys. Lett. **B252** (1990) 159.

[36] E. Maina, private communication.

$\tilde{y}$	$D_2(y)$- JADE	$D_2(y)$-P0	$1-T$
0.000 - 0.040	$1.023 \pm 0.005\ ^{+0.008}_{-0.008}$	$1.023 \pm 0.004\ ^{+0.007}_{-0.007}$	$0.943 \pm 0.010\ ^{+0.021}_{-0.017}$
0.040 - 0.050	$0.954 \pm 0.026\ ^{+0.051}_{-0.030}$	$0.933 \pm 0.027\ ^{+0.059}_{-0.031}$	$1.082 \pm 0.021\ ^{+0.042}_{-0.024}$
0.050 - 0.065	$1.011 \pm 0.025\ ^{+0.038}_{-0.044}$	$0.973 \pm 0.027\ ^{+0.040}_{-0.049}$	$1.150 \pm 0.021\ ^{+0.022}_{-0.080}$
0.065 - 0.080	$0.929 \pm 0.029\ ^{+0.032}_{-0.057}$	$0.938 \pm 0.030\ ^{+0.039}_{-0.043}$	$1.048 \pm 0.024\ ^{+0.023}_{-0.025}$
0.080 - 0.100	$0.911 \pm 0.029\ ^{+0.029}_{-0.033}$	$0.926 \pm 0.031\ ^{+0.033}_{-0.067}$	$0.987 \pm 0.024\ ^{+0.068}_{-0.023}$
0.100 - 0.140	$0.987 \pm 0.027\ ^{+0.030}_{-0.033}$	$0.932 \pm 0.028\ ^{+0.082}_{-0.030}$	$1.023 \pm 0.022\ ^{+0.028}_{-0.039}$
0.140 - 0.200	$0.936 \pm 0.031\ ^{+0.056}_{-0.039}$	$0.976 \pm 0.035\ ^{+0.041}_{-0.059}$	$0.993 \pm 0.026\ ^{+0.045}_{-0.036}$
> 0.200	$0.932 \pm 0.044\ ^{+0.051}_{-0.053}$	$0.964 \pm 0.047\ ^{+0.059}_{-0.051}$	$0.965 \pm 0.030\ ^{+0.039}_{-0.059}$
0.040 - 0.200	$0.956 \pm 0.012\ ^{+0.020}_{-0.019}$	$0.947 \pm 0.012\ ^{+0.024}_{-0.022}$	$1.044 \pm 0.010\ ^{+0.019}_{-0.018}$
Correlated error	$^{+0.013}_{-0.010}$	$^{+0.014}_{-0.010}$	$^{+0.012}_{-0.010}$
$\tilde{y}$	M_H^2/E_{vis}^2	M_D^2/E_{vis}^2	M_J^2/E_{vis}^2
0.000 - 0.040	$1.002 \pm 0.005\ ^{+0.011}_{-0.010}$	$1.020 \pm 0.004\ ^{+0.008}_{-0.008}$	$1.003 \pm 0.003\ ^{+0.007}_{-0.006}$
0.040 - 0.050	$1.040 \pm 0.023\ ^{+0.026}_{-0.054}$	$0.968 \pm 0.028\ ^{+0.037}_{-0.039}$	$1.039 \pm 0.020\ ^{+0.025}_{-0.040}$
0.050 - 0.065	$1.072 \pm 0.023\ ^{+0.029}_{-0.077}$	$0.947 \pm 0.026\ ^{+0.035}_{-0.034}$	$1.050 \pm 0.021\ ^{+0.024}_{-0.068}$
0.065 - 0.080	$0.988 \pm 0.026\ ^{+0.062}_{-0.026}$	$0.926 \pm 0.031\ ^{+0.041}_{-0.047}$	$0.996 \pm 0.025\ ^{+0.038}_{-0.026}$
0.080 - 0.100	$0.927 \pm 0.026\ ^{+0.031}_{-0.035}$	$0.899 \pm 0.032\ ^{+0.068}_{-0.036}$	$0.931 \pm 0.026\ ^{+0.029}_{-0.031}$
0.100 - 0.140	$0.924 \pm 0.025\ ^{+0.102}_{-0.032}$	$0.969 \pm 0.032\ ^{+0.032}_{-0.073}$	$0.900 \pm 0.024\ ^{+0.108}_{-0.030}$
0.140 - 0.200	$0.970 \pm 0.032\ ^{+0.042}_{-0.044}$	$0.901 \pm 0.038\ ^{+0.075}_{-0.049}$	$0.949 \pm 0.032\ ^{+0.047}_{-0.041}$
> 0.200	$1.011 \pm 0.047\ ^{+0.063}_{-0.206}$	$0.973 \pm 0.055\ ^{+0.068}_{-0.250}$	$0.988 \pm 0.047\ ^{+0.060}_{-0.183}$
0.040 - 0.200	$0.983 \pm 0.012\ ^{+0.021}_{-0.020}$	$0.941 \pm 0.013\ ^{+0.028}_{-0.024}$	$0.986 \pm 0.011\ ^{+0.019}_{-0.023}$
Correlated error	$^{+0.012}_{-0.007}$	$^{+0.021}_{-0.015}$	$^{+0.012}_{-0.017}$
χ	Σ_{EEC}		
30° - 45°	$1.031 \pm 0.008\ ^{+0.014}_{-0.015}$		
45° - 60°	$0.996 \pm 0.009\ ^{+0.014}_{-0.013}$		
60° - 75°	$0.976 \pm 0.009\ ^{+0.016}_{-0.015}$		
75° - 90°	$0.975 \pm 0.010\ ^{+0.015}_{-0.016}$		
90° - 105°	$0.985 \pm 0.011\ ^{+0.016}_{-0.015}$		
105° - 120°	$0.992 \pm 0.011\ ^{+0.013}_{-0.013}$		
120° - 135°	$0.989 \pm 0.010\ ^{+0.015}_{-0.015}$		
135° - 150°	$1.031 \pm 0.009\ ^{+0.018}_{-0.018}$		
45° - 135°	$0.986 \pm 0.004\ ^{+0.008}_{-0.007}$		
Correlated error	$^{+0.006}_{-0.004}$		

Table 1: The ratio of event shape variables for b events to those for all events, at the particle level. The first error is statistical and the second is the uncorrelated systematic error. The correlated error, discussed in section 4.2, is given separately.

distribution	$D_2(y)$-JADE	$D_2(y)$-P0	$1-T$	M_H^2/E_{vis}^2	M_D^2/E_{vis}^2	M_J^2/E_{vis}^2	$\Sigma_{EEC}(\chi)$
range of $\tilde{y}$	0.04–0.20	0.04–0.20	0.04–0.20	0.04–0.20	0.04–0.20	0.04–0.20	45°–135°
$\tau_b = 1.6$ ps	+0.002	+0.002	+0.001	+0.001	+0.002	< 0.001	+0.001
$\tau_b = 1.4$ ps	−0.002	−0.003	−0.001	−0.001	−0.003	< 0.001	−0.001
lifetime c hadrons	±0.002	±0.002	±0.001	±0.002	±0.002	±0.002	±0.001
B - multipl. −10%	+0.002	+0.001	−0.006	< 0.001	+0.009	+0.006	< 0.001
B - multipl. +10%	−0.005	−0.004	+0.005	−0.002	−0.012	−0.008	−0.001
C - multipl. −10%	+0.001	+0.001	< 0.001	< 0.001	+0.002	< 0.001	< 0.001
C - multipl. +10%	−0.001	−0.001	+0.001	< 0.001	−0.001	< 0.001	< 0.001
b tag efficiency +10%	+0.003	+0.003	+0.002	+0.003	+0.002	+0.002	+0.003
$\epsilon_b = +0.0095$	< 0.001	+0.002	+0.002	< 0.001	+0.001	−0.001	+0.002
$\epsilon_b = +0.0025$	+0.003	+0.002	+0.003	+0.004	+0.003	+0.005	−0.001
$\Gamma_{b\bar{b}} * 0.98$	−0.004	−0.004	−0.002	−0.004	−0.004	−0.006	−0.001
$\Gamma_{b\bar{b}} * 1.02$	+0.004	+0.004	+0.002	+0.004	+0.004	+0.006	+0.001
$\Gamma_{c\bar{c}} * 0.85$	−0.001	< 0.001	+0.001	< 0.001	+0.001	+0.002	+0.001
$\Gamma_{c\bar{c}} * 1.15$	−0.001	< 0.001	+0.001	< 0.001	+0.001	+0.002	+0.001
$(L/\sigma)^{\max} = \infty$	−0.003	−0.001	+0.003	+0.002	< 0.001	+0.001	< 0.001
$(L/\sigma)^{\max} = 30$	+0.009	+0.011	+0.008	+0.009	+0.013	+0.005	+0.003
$(L/\sigma)^{\min} = 5$	−0.002	−0.005	−0.004	−0.003	−0.006	−0.006	−0.001
$(L/\sigma)^{\min} = 0$	< 0.001	< 0.001	−0.001	< 0.001	< 0.001	< 0.001	< 0.001
Monte Carlo statistics	±0.011	±0.011	±0.009	±0.010	±0.012	±0.009	±0.004
procedure Σ_{EEC}	–	–	–	–	–	–	+0.004
tracking resolution $\beta = 1.2$	+0.005	+0.005	+0.004	+0.003	+0.005	−0.001	+0.003
tracking resolution $\beta = 1.4$	−0.005	−0.005	−0.004	−0.003	−0.005	+0.001	−0.003
detector correction	+0.005	+0.003	−0.006	−0.001	+0.012	−0.012	+0.001
$\epsilon_b = +0.0095$	+0.006	+0.005	−0.005	+0.001	+0.006	< 0.001	< 0.001
$\epsilon_b = +0.0025$	−0.013	−0.009	+0.002	−0.001	−0.008	+0.002	−0.004
1 GeV/$c^2 \leq Q_0 \leq$ 6 GeV/c^2	−0.005	−0.002	+0.017	−0.006	−0.012	−0.004	−0.002
total systematics	$^{+0.018}_{-0.018}$	$^{+0.019}_{-0.017}$	$^{+0.023}_{-0.014}$	$^{+0.016}_{-0.013}$	$^{+0.025}_{-0.023}$	$^{+0.017}_{-0.019}$	$^{+0.008}_{-0.008}$
statistics	0.011	0.012	0.009	0.010	0.012	0.009	0.004

Table 2: Summary of the systematic errors for the mean of the ratio $R^{\mathrm{b}}(\tilde{y})$, for all seven observables. They are valid for the results at parton level. The sign denotes the change in direction obtained for a given effect. When an effect was smaller than 0.0005 in either direction this is indicated by < 0.001 in the table. The range of $\tilde{y}$ used in the calculation of the mean is given in row 2.

Variable	x_μ^{opt}
$D_2(y)$-JADE	0.069
$D_2(y)$-P0	0.250
$1-T$	0.041
M_H^2/E_{vis}^2	0.070
M_D^2/E_{vis}^2	0.093
M_J^2/E_{vis}^2	0.070
Σ_{EEC}	0.160

Table 3: Optimized renormalisation scales, x_μ^{opt}, for all observables, as used in the analysis.

		$\mathcal{O}(\alpha_s)$	LLA	average
distribution	fit range	$\alpha_s^{\rm b}/\alpha_s^{\rm incl}$	$\alpha_s^{\rm b}/\alpha_s^{\rm incl}$	$\alpha_s^{\rm b}/\alpha_s^{\rm incl}$
$D_2(y)$-JADE	$0.04-0.20$	$1.016 \pm 0.010\ ^{+0.014}_{-0.020}$	$0.996 \pm 0.010\ ^{+0.014}_{-0.018}$	$1.006 \pm 0.010\ ^{+0.017}_{-0.021}$
$D_2(y)$-P0	$0.04-0.20$	$1.000 \pm 0.012\ ^{+0.018}_{-0.019}$	$0.980 \pm 0.012\ ^{+0.018}_{-0.018}$	$0.990 \pm 0.012\ ^{+0.021}_{-0.021}$
$1-T$	$0.04-0.20$	$0.986 \pm 0.008\ ^{+0.031}_{-0.015}$	$1.010 \pm 0.008\ ^{+0.024}_{-0.025}$	$0.998 \pm 0.008\ ^{+0.026}_{-0.022}$
M_H^2/E_{vis}^2	$0.04-0.20$	$0.981 \pm 0.011\ ^{+0.021}_{-0.014}$	$0.998 \pm 0.011\ ^{+0.025}_{-0.015}$	$0.990 \pm 0.011\ ^{+0.025}_{-0.017}$
M_D^2/E_{vis}^2	$0.04-0.20$	$0.999 \pm 0.014\ ^{+0.024}_{-0.027}$	$0.985 \pm 0.014\ ^{+0.026}_{-0.028}$	$0.993 \pm 0.014\ ^{+0.026}_{-0.027}$
M_J^2/E_{vis}^2	$0.04-0.20$	$0.967 \pm 0.009\ ^{+0.023}_{-0.019}$	$0.985 \pm 0.009\ ^{+0.024}_{-0.019}$	$0.976 \pm 0.009\ ^{+0.025}_{-0.021}$
Σ_{EEC}	$45^\circ - 135^\circ$	$0.995 \pm 0.003\ ^{+0.008}_{-0.011}$	$0.996 \pm 0.003\ ^{+0.010}_{-0.014}$	$0.995 \pm 0.003\ ^{+0.008}_{-0.012}$

Table 4: A summary of the ratio $\alpha_s^{\rm b}/\alpha_s^{\rm incl}$ for all variables. Given are the $\tilde{y}$ range used in the fit (second column), the results for the mass correction based on the $\mathcal{O}(\alpha_s)$ calculation (third column), those based on parton shower calculations (fourth column), and the average of the two mass corrections as discussed in the text (last column). These results are also shown in figure 4. The errors are the statistical and systematic errors.

distribution	$D_2(y)$-JADE	$D_2(y)$-P0	$1-T$	M_H^2/E_{vis}^2	M_D^2/E_{vis}^2	M_J^2/E_{vis}^2	$\Sigma_{EEC}(\chi)$
range of $\tilde{y}$	0.04–0.20	0.04–0.20	0.04–0.20	0.04–0.20	0.04–0.20	0.04–0.20	45°–135°
$\tau_b = 1.6$ ps	$+0.001$	$+0.002$	$+0.001$	$+0.001$	$+0.002$	< 0.001	$+0.001$
$\tau_b = 1.4$ ps	-0.002	-0.003	-0.001	-0.001	-0.003	< 0.001	-0.001
lifetime c hadrons	± 0.002	± 0.002	± 0.001	± 0.002	± 0.002	± 0.002	± 0.001
B - multipl. -10%	$+0.001$	< 0.001	-0.004	< 0.001	$+0.008$	$+0.005$	< 0.001
B - multipl. $+10\%$	-0.005	-0.004	$+0.004$	-0.001	-0.012	-0.006	-0.001
C - multipl. -10%	$+0.001$	$+0.001$	< 0.001	$+0.001$	$+0.002$	< 0.001	< 0.001
C - multipl. $+10\%$	-0.001	-0.001	$+0.001$	< 0.001	-0.001	$+0.001$	< 0.001
b tag efficiency $+10\%$	$+0.003$	$+0.003$	$+0.002$	$+0.003$	$+0.002$	$+0.001$	$+0.003$
$\epsilon_b = +0.0095$	< 0.001	$+0.002$	$+0.001$	< 0.001	$+0.001$	-0.001	$+0.002$
$\epsilon_b = +0.0025$	$+0.002$	$+0.002$	$+0.003$	$+0.004$	$+0.003$	$+0.004$	-0.001
$\Gamma_{b\bar{b}} * 0.98$	-0.003	-0.004	-0.002	-0.003	-0.004	-0.005	-0.001
$\Gamma_{b\bar{b}} * 1.02$	$+0.003$	$+0.004$	$+0.002$	$+0.003$	$+0.004$	$+0.005$	$+0.001$
$\Gamma_{c\bar{c}} * 0.85$	< 0.001	< 0.001	$+0.001$	$+0.001$	$+0.001$	$+0.001$	$+0.001$
$\Gamma_{c\bar{c}} * 1.15$	< 0.001	< 0.001	$+0.001$	$+0.001$	$+0.001$	$+0.001$	$+0.001$
$(L/\sigma)^{max} = \infty$	-0.002	-0.001	$+0.002$	$+0.003$	< 0.001	$+0.002$	< 0.001
$(L/\sigma)^{max} = 30$	$+0.007$	$+0.010$	$+0.007$	$+0.008$	$+0.012$	$+0.004$	$+0.003$
$(L/\sigma)^{min} = 5$	-0.002	-0.005	-0.003	-0.003	-0.006	-0.005	-0.002
$(L/\sigma)^{min} = 0$	< 0.001	< 0.001	-0.001	$+0.001$	< 0.001	-0.001	< 0.001
Monte Carlo statistics	± 0.010	± 0.012	± 0.008	± 0.010	± 0.014	± 0.009	± 0.003
procedure Σ_{EEC}	–	–	–	–	–	–	$+0.003$
tracking resolution $\beta = 1.2$	$+0.004$	$+0.005$	$+0.003$	$+0.003$	$+0.005$	-0.001	$+0.003$
tracking resolution $\beta = 1.4$	-0.004	-0.005	-0.003	-0.003	-0.005	$+0.001$	-0.003
Detector correction	$+0.004$	< 0.001	-0.005	-0.006	$+0.011$	-0.013	< 0.001
$\epsilon_b = +0.0095$	$+0.005$	$+0.005$	-0.004	$+0.001$	$+0.006$	< 0.001	< 0.001
$\epsilon_b = +0.0025$	-0.011	-0.009	$+0.001$	-0.001	-0.008	$+0.002$	-0.004
1 GeV/$c^2 \leq Q_0 \leq$ 6 GeV/c^2	-0.004	-0.002	$+0.014$	-0.005	-0.012	-0.004	-0.003
scale	-0.002	< 0.001	$+0.012$	$+0.017$	-0.006	$+0.019$	$+0.001$
$m_b = 4.5$ GeV/c^2	-0.007	-0.007	-0.011	$+0.002$	-0.002	$+0.002$	-0.009
RMS parton showers	± 0.001	± 0.002	± 0.008	± 0.003	± 0.005	± 0.003	± 0.003
mass correction	± 0.010	± 0.010	∓ 0.012	∓ 0.008	∓ 0.007	∓ 0.009	< 0.001
total systematics	$^{+0.017}_{-0.021}$	$^{+0.021}_{-0.021}$	$^{+0.026}_{-0.022}$	$^{+0.025}_{-0.017}$	$^{+0.026}_{-0.027}$	$^{+0.025}_{-0.021}$	$^{+0.008}_{-0.012}$
statistics	0.010	0.012	0.008	0.011	0.014	0.009	0.003

Table 5: Summary of the systematic errors for the ratio $\alpha_s^{\rm b}/\alpha_s^{\rm incl}$, as obtained with the average mass correction. The sign denotes the change in direction obtained for a given effect. When an effect was smaller than 0.0005 in either direction this is indicated by < 0.001 in the table. The $\tilde{y}$ range used for the α_s determination is given in row 2.

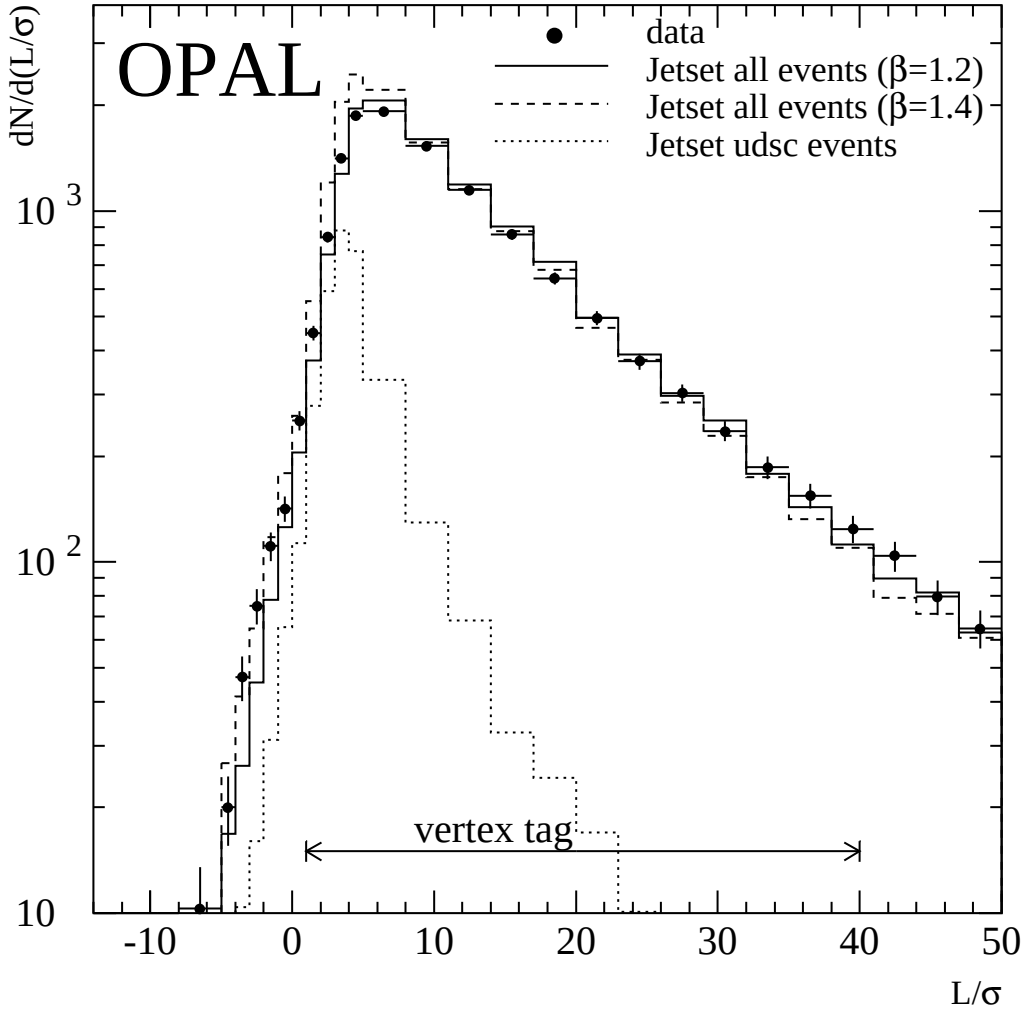

Figure 1: Decay length distribution, L/σ, for the data (full points), JETSET all flavours with a smearing factor $\beta = 1.2$ (full line), JETSET all flavours for $\beta = 1.4$ (dashed line), and JETSET udsc contribution (dotted line). For JETSET, a b lifetime of 1.5 ps was assumed and the charged multiplicity of b hadrons, as measured in the detector, was increased by 10%, relative to that obtained with the standard parameters. The JETSET events were normalized to the data after selection cuts. The vertex tag region used for the main result is indicated at the bottom.

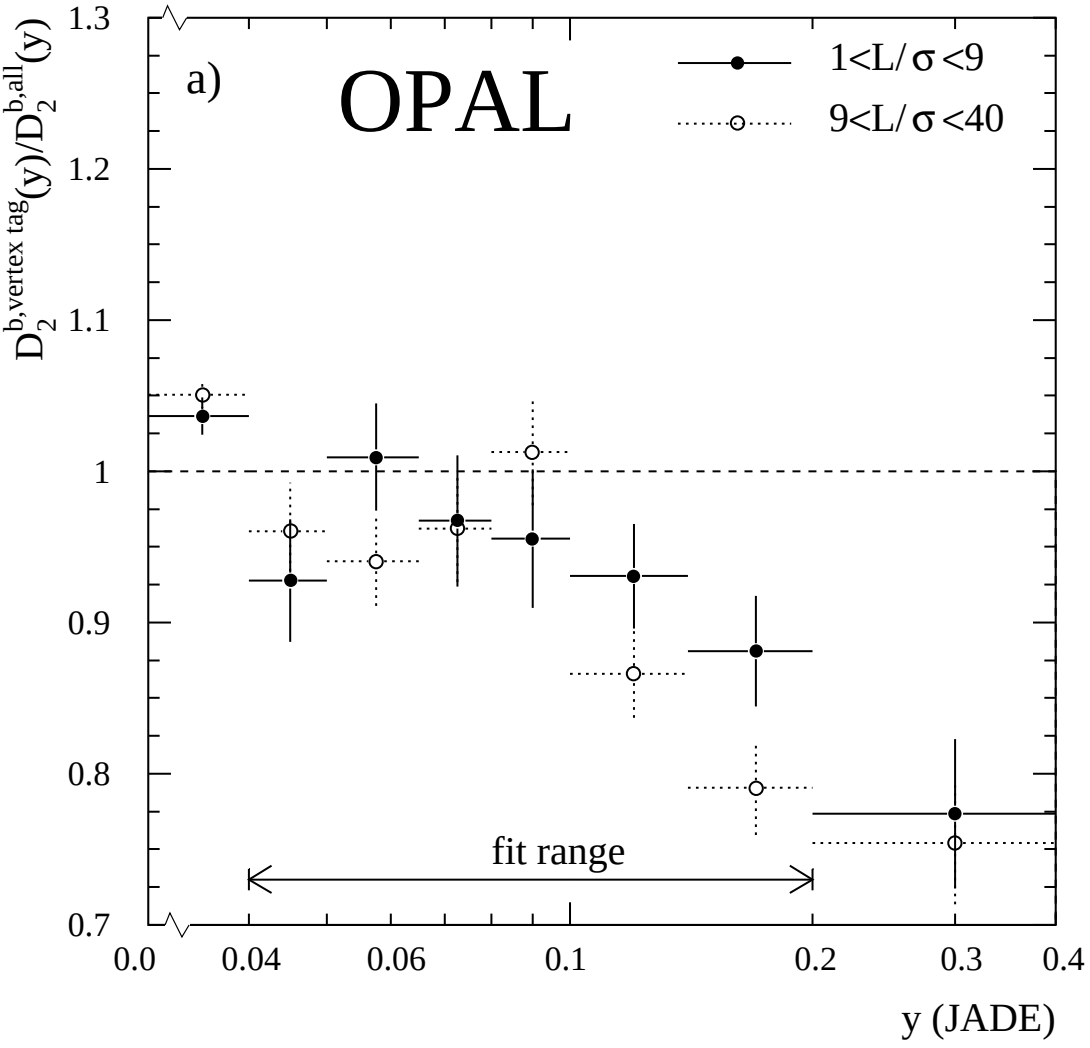

Figure 2: Bias introduced by the vertex tag requirement on the variable y(JADE) (Fig. 2a). The quantity plotted is the ratio, as obtained with JETSET, of the differential jet rate for the b events satisfying a vertex tag and the differential jet rate for all b events versus y(JADE) for a vertex tag $1.0 < L/\sigma < 9.0$ (solid points) and for a vertex tag $9.0 < L/\sigma < 40.0$ (open points). Fig. 2b shows the bias introduced for the variable Σ_{EEC}. Plotted is the ratio $\Sigma_{EEC}^{b,\ vertex\ tag}(\chi)/\Sigma_{EEC}^{b,\ all}(\chi)$ versus the angle χ.

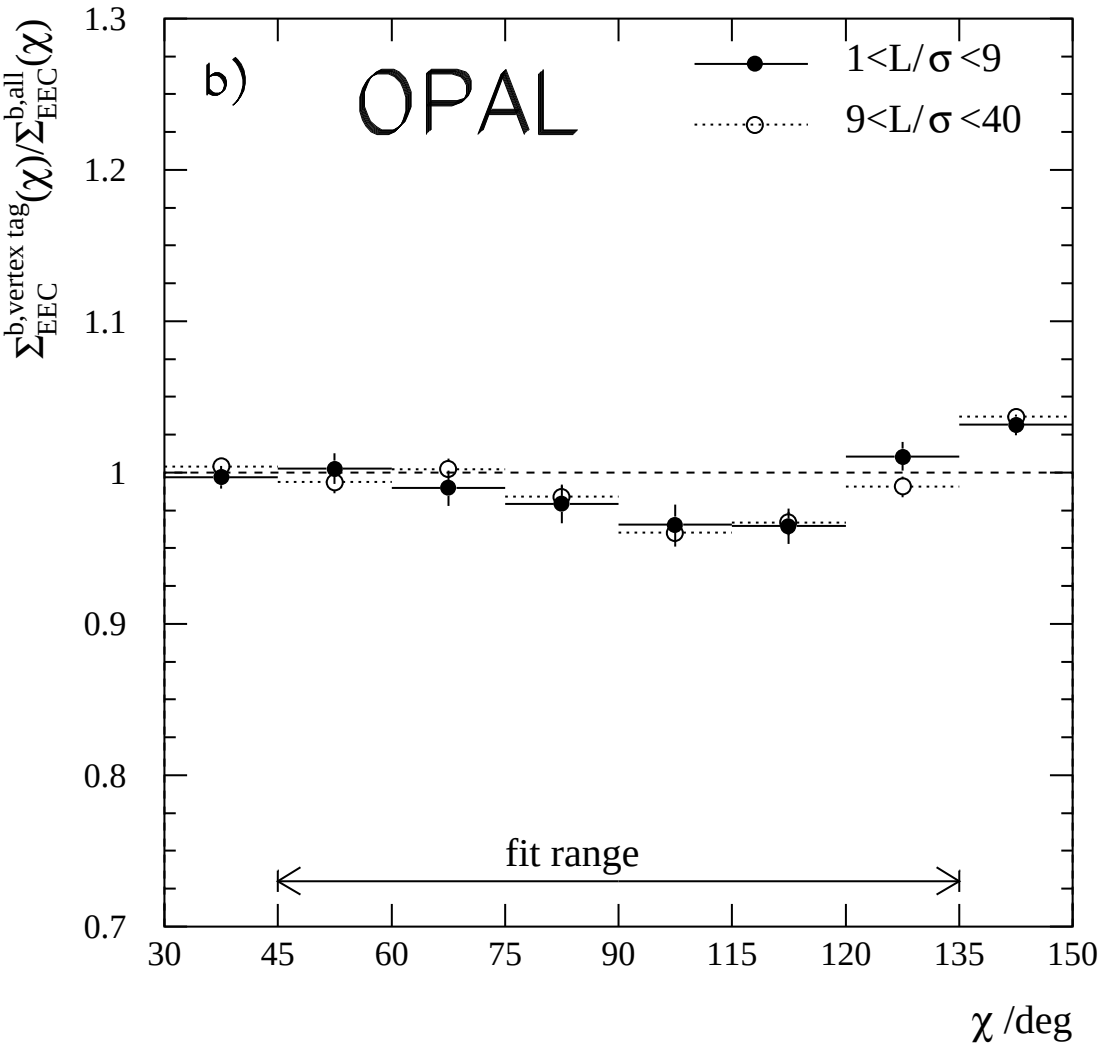
b)
OPAL
1<L/σ<9
9<L/σ<40
fit range
$\Sigma^{b,vertex\ tag}_{EEC}(\chi)/\Sigma^{b,all}_{EEC}(\chi)$
χ /deg
1.3
1.2
1.1
1
0.9
0.8
0.7
30
45
60
75
90
115
120
135
150

Fig. 2b

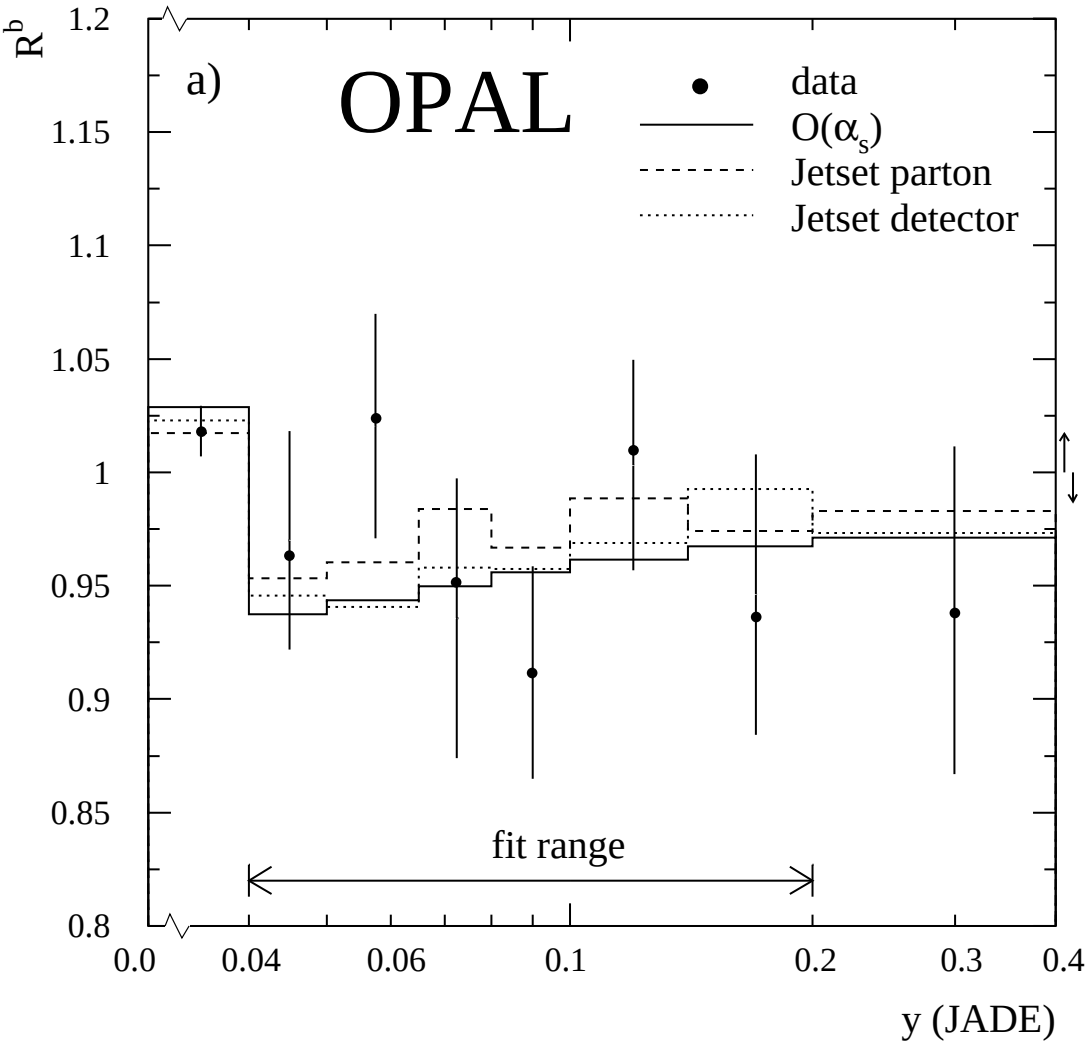

Figure 3: The ratio of event shape distributions for b quark events to those for all events for a) $D_2(y)$–JADE, b) $D_2(y)$–P0, c) $1-T$, d) M_H^2/E_{vis}^2, e) M_D^2/E_{vis}^2, f) M_J^2/E_{vis}^2 and g) $\Sigma_{EEC}(\chi)$. The full points with error bars are the data, corrected for detector and fragmentation effects. The errors shown are the statistical and uncorrelated systematic errors, added in quadrature. The correlated error, by which all points within the fit range can be shifted simultaneously, is indicated by arrows at the right side of the figure. In addition, the predictions of the $\mathcal{O}(\alpha_s)$ calculation for b quarks is given (full line) as well as those of JETSET at the parton level (dashed line) and after full detector simulation (dotted line). In figs a - f, the first bin does not contain independent information and its value is given by the normalisation.

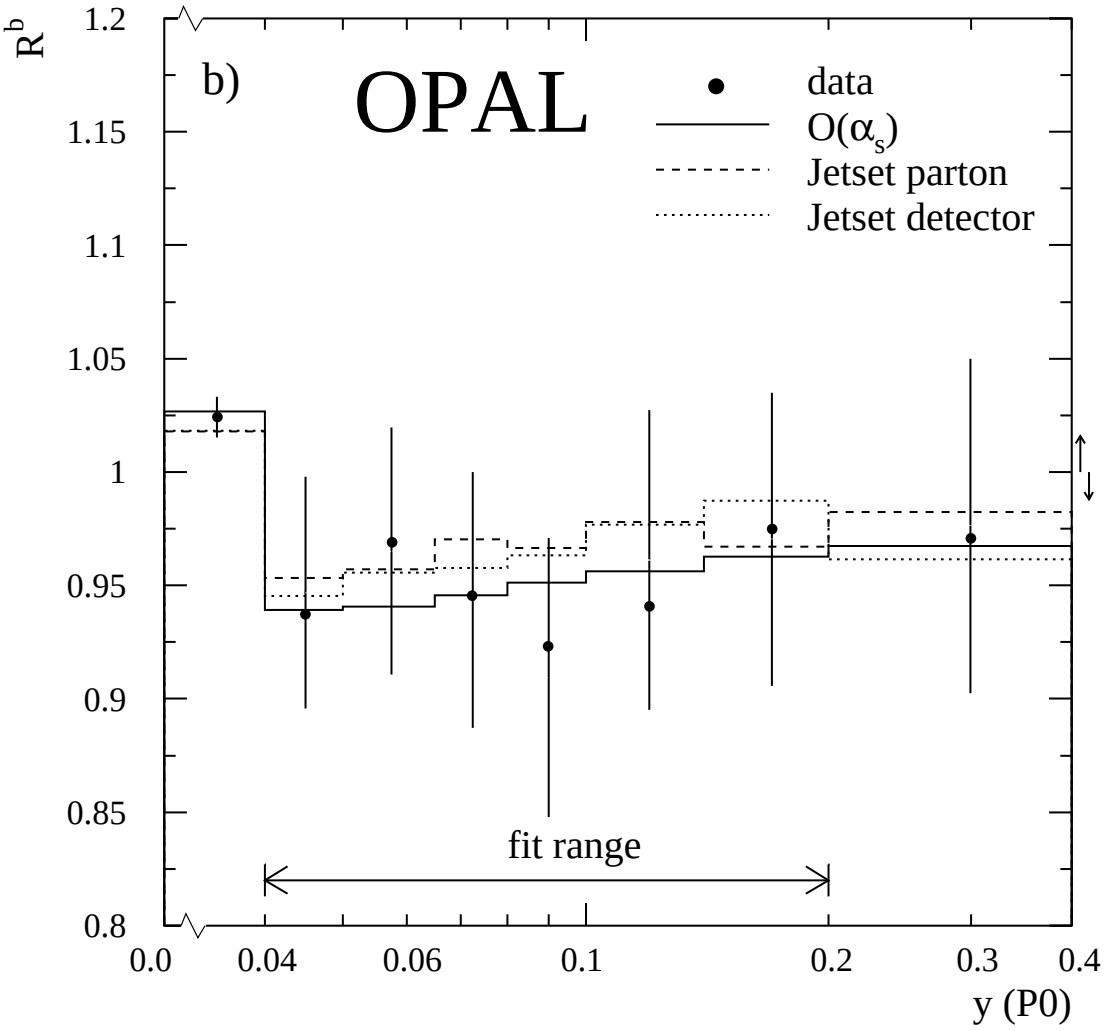
R^b
b)
OPAL
data
$O(\alpha_s)$
Jetset parton
Jetset detector
fit range
1.2
1.15
1.1
1.05
1
0.95
0.9
0.85
0.8
0.0
0.04
0.06
0.1
0.2
0.3
0.4
y (P0)

Fig. 3b

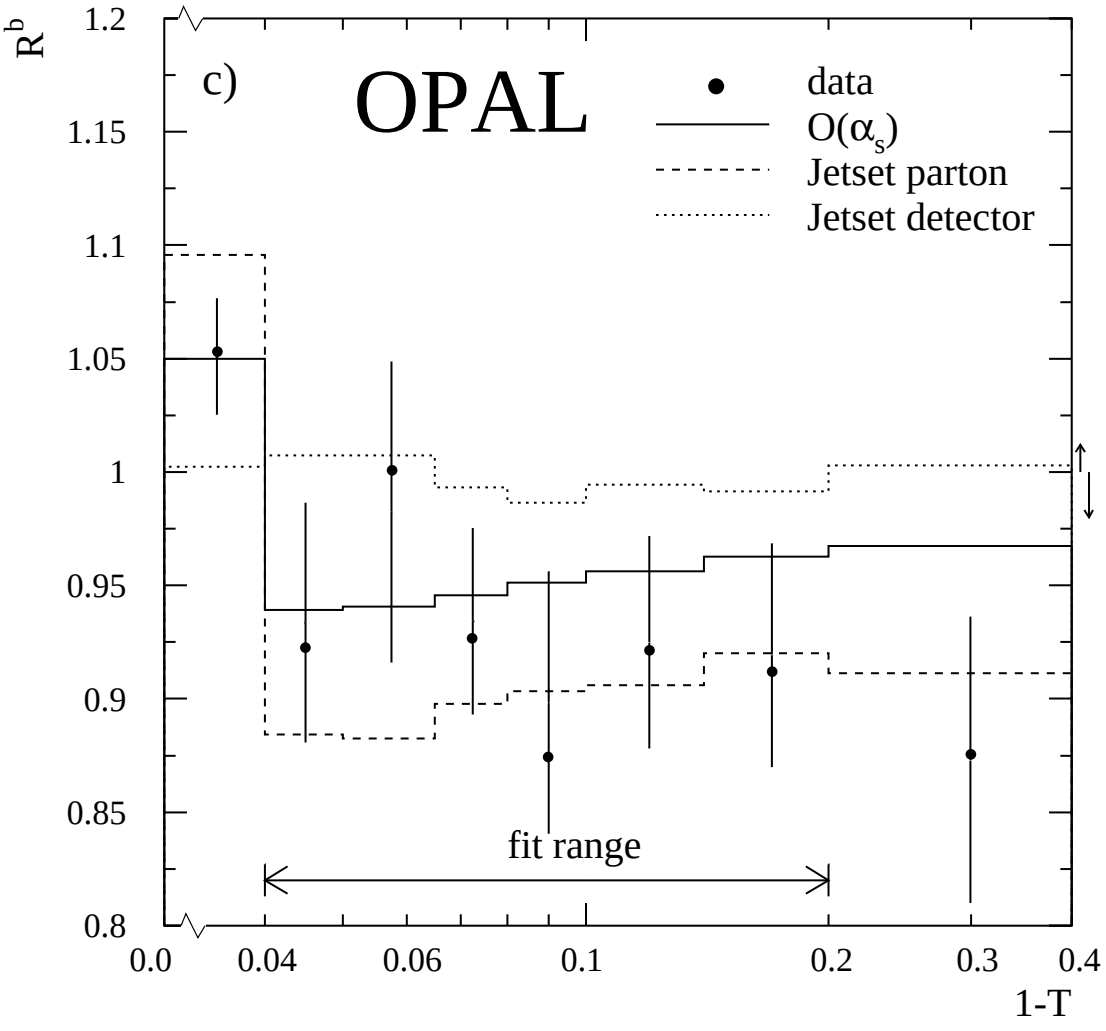
c)
OPAL
data
O(α_s)
Jetset parton
Jetset detector
R^b
1.2
1.15
1.1
1.05
1
0.95
0.9
0.85
0.8
0.0
0.04
0.06
0.1
0.2
0.3
0.4
1-T
fit range

Fig. 3c

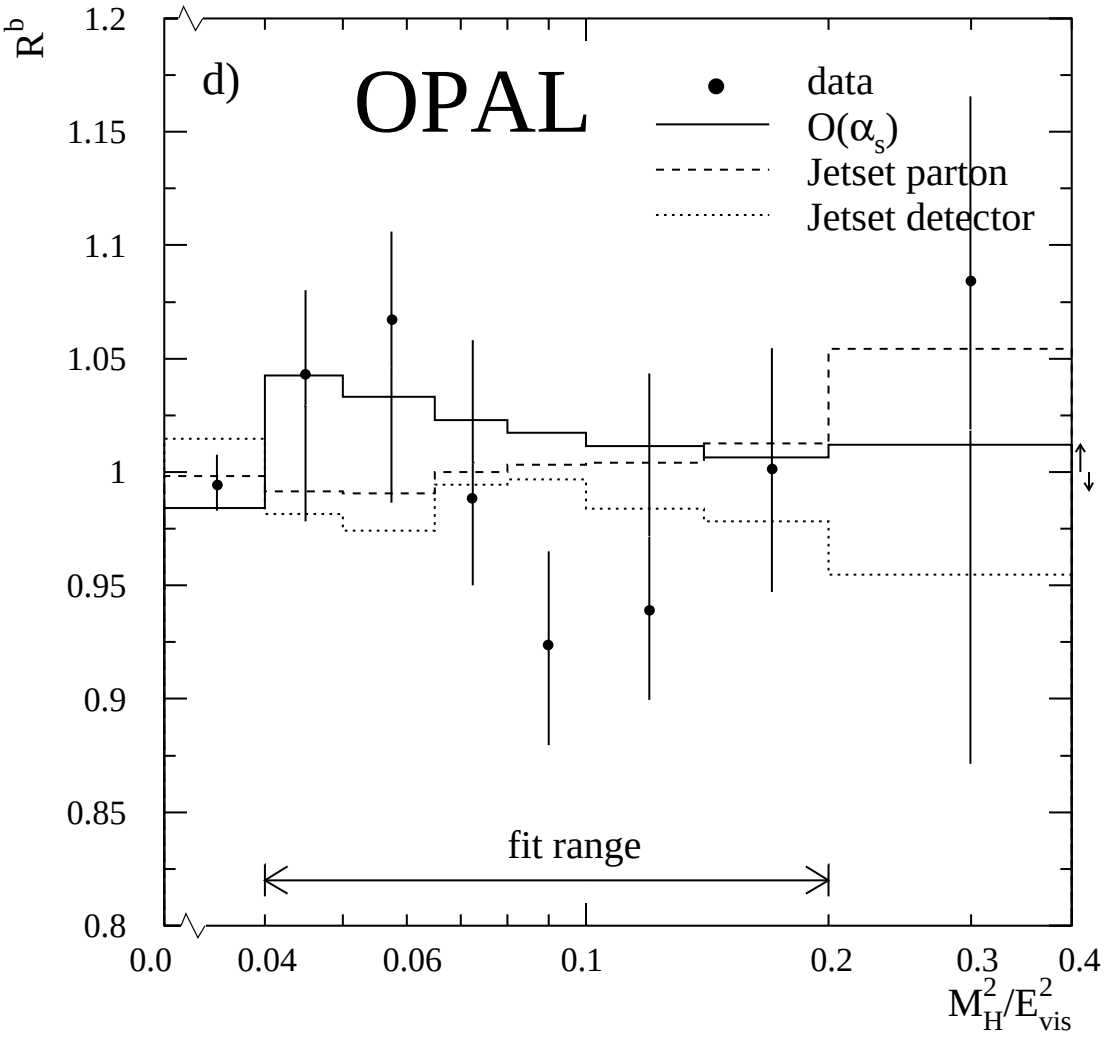
d)
OPAL
data
O(α_s)
Jetset parton
Jetset detector
R^b
1.2
1.15
1.1
1.05
1
0.95
0.9
0.85
0.8
0.0
0.04
0.06
0.1
0.2
0.3
0.4
fit range
M_H^2/E_vis^2

Fig. 3d

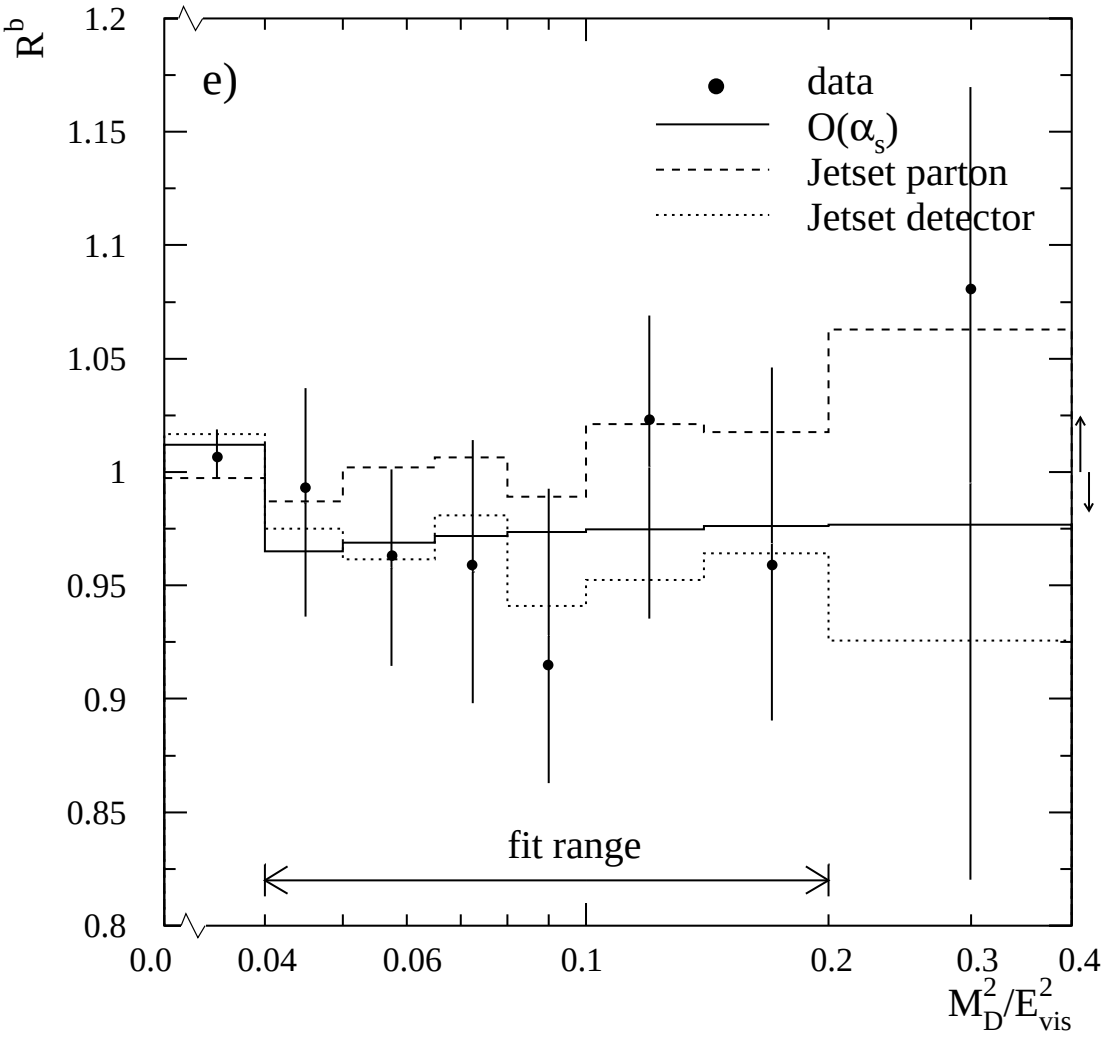
R^b
e)
data
$O(\alpha_s)$
Jetset parton
Jetset detector
fit range
1.2
1.15
1.1
1.05
1
0.95
0.9
0.85
0.8
0.0
0.04
0.06
0.1
0.2
0.3
0.4
M_D^2/E_{vis}^2

Fig. 3e

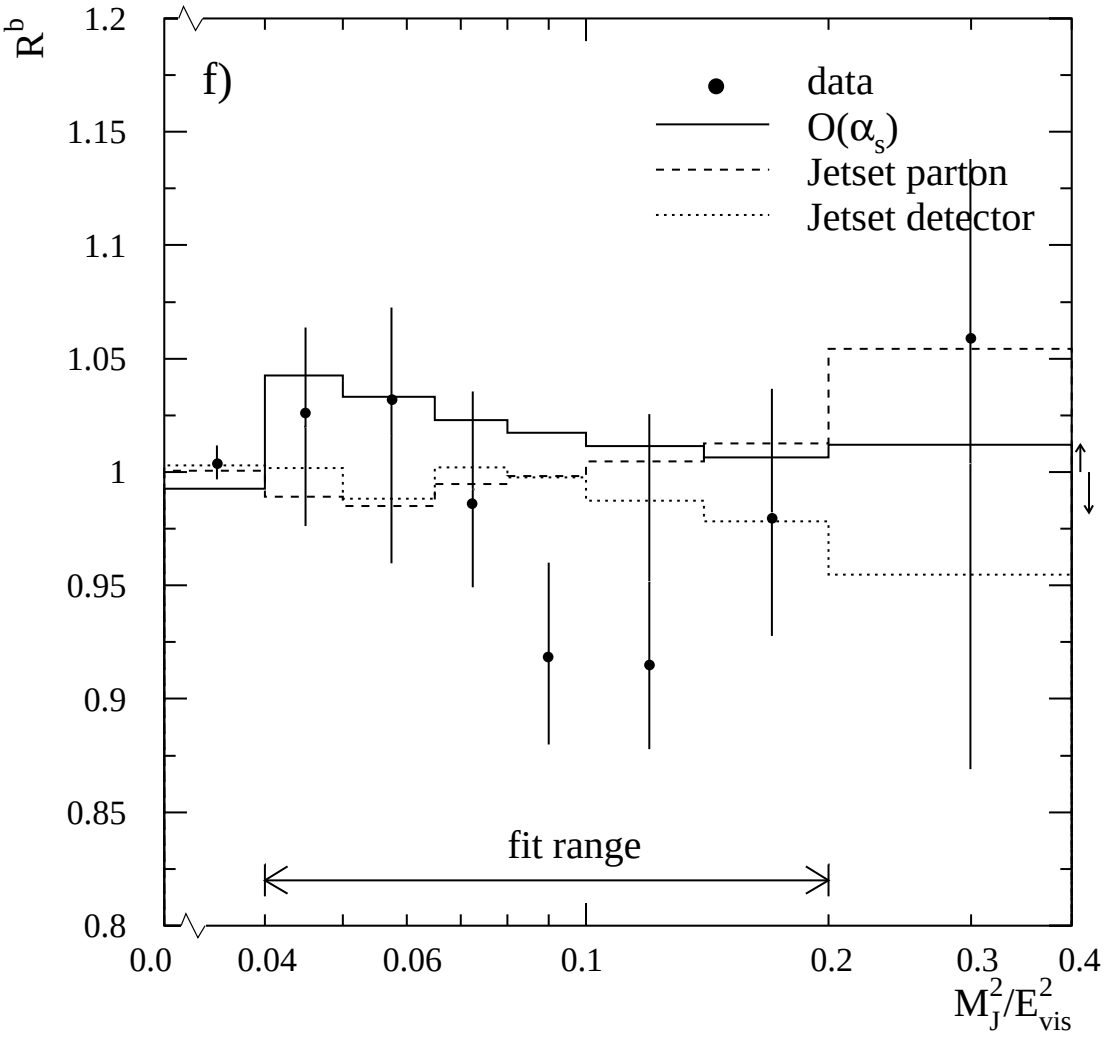
f)
data
O(α_s)
Jetset parton
Jetset detector
R^b
1.2
1.15
1.1
1.05
1
0.95
0.9
0.85
0.8
0.0
0.04
0.06
0.1
0.2
0.3
0.4
fit range
M_J^2/E_vis^2

Fig. 3f

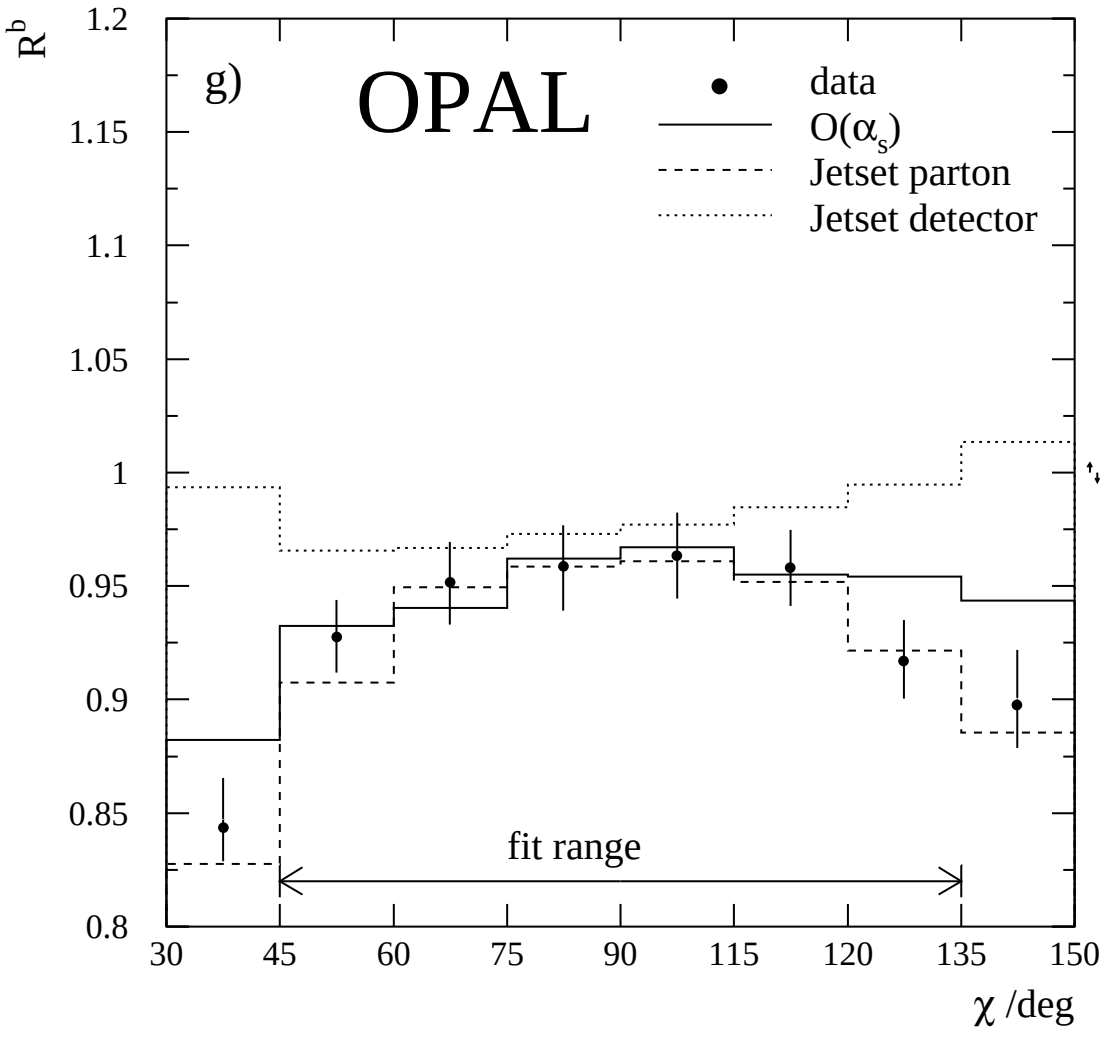
g)
OPAL
data
O(α_s)
Jetset parton
Jetset detector
R^b
1.2
1.15
1.1
1.05
1
0.95
0.9
0.85
0.8
fit range
30
45
60
75
90
115
120
135
150
χ /deg

Fig. 3g

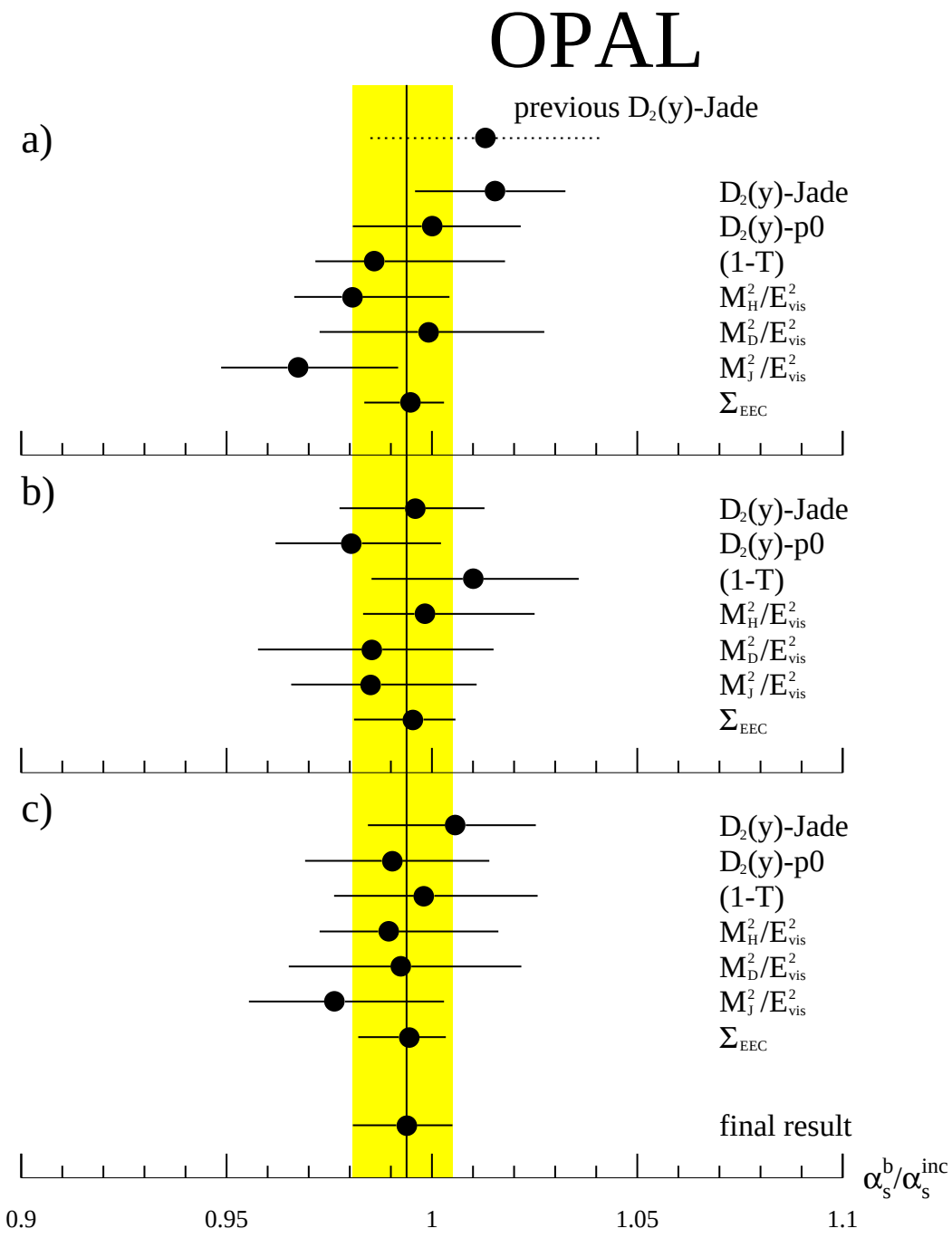

Figure 4: The ratio $\alpha_s^{\rm b}/\alpha_s^{\rm incl}$, for various ways to take mass effects into account. The errors include the systematic error. a) Mass correction based on the $\mathcal{O}(\alpha_s)$ calculation; the point with the dashed error bar is our previous result (ref.[5]), b) mass correction based on parton shower calculations, c) average of a) and b), for details see text. The final average result is given at the bottom and is indicated by the shaded band.